NASA TECHNICAL MEMORANDUM

NASA TM X-2027

NASA TM X-2027

PERFORMANCE OF AN AUXILIARY INLET EJECTOR NOZZLE WITH FIXED DOORS AND SINGLE-HINGE TRAILING-EDGE FLAP

by Albert L. Johns and Fred W. Steffen

Lewis Research Center

Cleveland, Ohio 44135

NATIONAL AERONAUTICS AND SPACE ADMINISTRATION • WASHINGTON, D. C. • JUNE 1970

1. Report No. NASA TM X-2027	2. Government Accession No.	3. Recipient's Catalog No.
4. Title and Subtitle PERFORMANCE OF AN AUXILIARY INLET EJECTOR NOZZLE WITH FIXED DOORS AND SINGLE-HINGE TRAILING-EDGE FLAP		5. Report Date June 1970 6. Performing Organization Code
7. Author(s) Albert L. Johns and Fred W. Steffen		8. Performing Organization Report No. E-5502
9. Performing Organization Name and Address Lewis Research Center National Aeronautics and Space Administration Cleveland, Ohio 44135		10. Work Unit No. 126-15 11. Contract or Grant No.
12. Sponsoring Agency Name and Address National Aeronautics and Space Administration Washington, D.C. 20546		13. Type of Report and Period Covered Technical Memorandum 14. Sponsoring Agency Code
15. Supplementary Notes		

16. Abstract

An auxiliary inlet ejector nozzle applicable to a supersonic-cruise aircraft was evaluated over a range of free-stream Mach numbers from 0 to 1.20 at appropriate nozzle pressure ratios. Two primary throat areas were used: one to simulate nonreheat operation, and the other for reheat operation. The fixed-geometry shroud was only used in the closed position. The projected boattail area was 47 percent of the simulated nacelle area. Variation in auxiliary inlets included door type (single and double hinge) and values of tertiary flow area (controlled with fixed-position doors) from 0 to 71.5 percent of the shroud exit area. A slightly higher nozzle efficiency was obtained with the double-hinge doors at subsonic-cruise power setting, while the single-hinge doors were a little better at dry-acceleration power setting. At the reheat power setting, the maximum nozzle efficiency was obtained with the doors closed at Mach 0.60 and higher.

17. Key Words (Suggested by Author(s))	18. Distribution Statement
Propulsion Nozzle	Unclassified - unlimited

19. Security Classif. (of this report)	20. Security Classif. (of this page)	21. No. of Pages	22. Price*
Unclassified	Unclassified	60	$3.00

*For sale by the Clearinghouse for Federal Scientific and Technical Information Springfield, Virginia 22151

CONTENTS

PERFORMANCE OF AN AUXILIARY INLET EJECTOR NOZZLE WITH FIXED DOORS AND SINGLE-HINGE TRAILING-EDGE FLAP

by Albert L. Johns and Fred W. Steffen

Lewis Research Center

SUMMARY

An experimental investigation was conducted in the 8- by 6-Foot Supersonic Wind Tunnel to determine the performance characteristics of an auxiliary inlet ejector nozzle at free-stream Mach numbers from 0 to 1.20. The ejector nozzle incorporated a single-hinge trailing-edge flap fixed in the subsonic-cruise position with double- and single-hinge auxiliary inlet doors. The projected boattail area was 47 percent of the simulated nacelle area. Nozzle pressure ratio was varied from approximately 1.9 to 9.0. Corrected secondary weight flow from 0 to 16 percent of the primary nozzle flow was investigated.

Auxiliary inlets with fixed-position doors providing tertiary flow area equal to 71.5, 58.4, 36.8, and zero percent of the shroud exit area were tested. Two different primary throat areas were used: one to simulate nonreheat operation and the other for maximum reheat operation. Data are presented for pressure ratios which are typical of an afterburning turbojet engine in a supersonic-cruise aircraft. A nominal corrected secondary-weight-flow-rate ratio of 4 percent was used.

In general, overexpansion losses could be reduced at subsonic-cruise and dry-acceleration conditions by increasing the tertiary-inlet- to nozzle-exit-area ratio from 0 to 0.584. For maximum reheat acceleration, the primary jet was near full expansion at Mach numbers of 0.60 and higher, and, hence, the closed-door configuration offered the highest nozzle efficiency.

For subsonic cruise at Mach 0.90, peak nozzle efficiency of 89.7 percent was obtained with a double-hinge door configuration having a tertiary-inlet- to nozzle-exit-area ratio of 0.584. Peak nozzle efficiencies at takeoff were 99 percent for dry acceleration and 94.3 percent for maximum reheat acceleration. At the latter condition, the converging single-hinge aft flap caused a substantial loss in performance. With fixed-position open auxiliary inlets, a floating single-hinge trailing-edge flap would be on the inner-stop position only during a dry acceleration.

INTRODUCTION

As part of an extensive program in airbreathing propulsion, the Lewis Research Center is evaluating various exhaust nozzle concepts appropriate for supersonic-cruise aircraft. Ideally, these nozzles should operate efficiently over a wide range of flight conditions and engine-power settings. Such requirements will usually necessitate extensive variations in ejector-nozzle geometry, including both the primary nozzle and shroud exit areas. The performance of a variable-flap ejector and a low-angle plug nozzle designed for an afterburning turbojet engine in a supersonic-cruise aircraft is reported in references 1 and 2. Another nozzle type of interest is the auxiliary inlet ejector (ref. 3). At low power settings, auxiliary inlets open to admit tertiary air to prevent overexpansion of the primary jet. Hence, there is a reduced requirement for exit-area variation and a corresponding reduction in boattail angle and projected area.

This report documents the aerodynamic performance of an auxiliary inlet ejector with a single-hinge flap fixed in a subsonic position. The single-hinge flap ejector has an internal area ratio (A_9/A_8) of 1.99 for the nonreheat operation and 1.42 for reheat operation. The model had an 8.5-inch (21.59-cm) diameter and was tested in the 8- by 6-Foot Supersonic Wind Tunnel at Mach numbers from 0 to 1.20 and over a range of nozzle pressure ratios from 1.9 to 9.0. Corrected secondary weight flow was varied from 0 to 16 percent of the primary nozzle weight flow. The configurations were tested at power settings representing subsonic cruise, dry acceleration, and maximum reheat acceleration. The primary nozzle was simulated on the basis of a General Electric J85-GE-13 afterburning turbojet engine. Dry air at room temperature was used for both primary and secondary weight flows.

APPARATUS AND PROCEDURE

Installation in Wind Tunnel

A schematic view of the model support system in the 8- by 6-Foot Supersonic Wind Tunnel showing the internal geometry and thrust-measuring system is presented in figure 1. (Symbols are defined in appendix A.) The grounded portion of the model was supported from the tunnel ceiling by a vertical strut. The floating portion was attached to the primary and secondary air bottles which were cantilevered by flow tubes from external supply manifolds. The primary air bottle was supported by front and rear bearings. The secondary air passed through an annulus around the primary nozzle. The axial force of the nozzle, which included secondary and tertiary flow effects, was transmitted to the load cell located in the nose of the model. Since the floating portion of the

model included the afterbody and boattail, the measured force was that resulting from the interaction of the internal and external flows. General flow characteristics of this jet-exit model are described in reference 4.

Force Measurements

Both primary and secondary flow rates were measured by means of standard ASME flowmetering orifices located in the external supply lines. Thrust-minus-drag measurements were obtained from a load-cell readout of the axial forces acting on the floating portion of the model. Internal tare forces, determined by internal areas and measured tare pressures located as shown in figure 1, were accounted for in the thrust calculation.

A static calibration of the thrust-measuring system was obtained by applying known forces to the nozzle and measuring the output of the load cell. A water-cooled jacket surrounded the load cell and maintained a constant temperature of 90° F to eliminate errors in the calibration caused by variations in temperature from aerodynamic heating. The only external friction drag charged to the nozzle is that downstream of station 122.84 inches (312 cm, fig. 1). That force acting on the portion of the nozzle between stations 93.65 inches (238 cm) and 122.84 inches (312 cm) was measured on the load cell; however, it is not considered to be part of the nozzle drag. Its magnitude was estimated by using the semiempirical flat-plate mean skin friction coefficient given in figure 7 of reference 5 as a function of free-stream Mach number and Reynolds number. Previous measurements of the boundary-layer characteristics at the aft end of this jet-exit model in the 8- by 6-Foot Supersonic Wind Tunnel (ref. 6) indicated that the profile and thickness were essentially the same as those computed for a flat plate of equal length. The strut wake appeared to affect only a localized region near the top of the model and resulted in a slightly lower local free-stream velocity than measured on the side and bottom of the model. Therefore, the results of reference 5 were used without correction for three-dimensional flow effects or strut-interference effects.

A choke plate and two screens were utilized to give a good profile to the internal flow approaching the nozzle inlet. The ideal jet thrust for both the primary and secondary flow was calculated from the measured mass-flow rate expanded from its measured total pressure (P_7 and P_s, respectively) to p_0. Provision was made to equate the ideal thrust of the secondary flow to zero if its total pressure was less than p_0. Review of the data showed that this situation did occur. Hence, tailed data are used to designate such results. Nozzle efficiency is defined as the ratio of the measured gross thrust minus drag to the ideal gross thrust of the primary and secondary flows:

$$\text{Nozzle efficiency} = \frac{F - D}{F_{i,p} + F_{i,s}}$$

In addition to the nozzle efficiency, the data are also presented (appendix B) in the form of nozzle gross-thrust coefficient $(F - D)/F_{i,p}$.

Nozzle Configurations

A General Electric J85-GE-13 primary nozzle mechanism was simulated for this test, as illustrated in figure 2. Two different throat areas were used with each auxiliary inlet configuration in this test. The smaller throat area simulated nonreheat operation (primary nozzle configuration I), while the larger area simulated reheat operation (primary nozzle configuration II). The actuating mechanism blockage was simulated by a ring containing 12 slots. Secondary air was diverted through these slots by means of a deflector to simulate primary flap cooling air. Data were corrected to an average flow coefficient C_{D8} of 0.977 ($\alpha = 13.25^{\circ}$) for primary I and 0.985 ($\alpha = 5.3^{\circ}$) for primary II.

Basic dimensions and pertinent parameters are shown in figure 3 for the single-hinge trailing-edge flap. The flap length ratios L/d_8 with primary nozzle configurations I and II were 2.16 and 1.91, respectively. The nozzle spacing ratio s/d_8 was 0.585 with primary I and 0.575 with primary II. The projected boattail area A_β was 47 percent of the simulated nacelle area A_{max} with a boattail angle of 15°. The fixed-geometry shroud used during this test represented a fully closed flap position for subsonic-cruise operation. Figure 4(a) shows the basic dimensions and pertinent parameters for the auxiliary inlets. In each auxiliary inlet configuration, the 16 doors were simulated by a continuous ring with 16 equally spaced ribs welded to the upstream surfaces. The closed-door configuration contained no ribs. The total tertiary-flow-area to exit-area ratio A_{ter}/A_9 varied from 0 (closed doors) to 0.715 (20° and 10°-20° doors).

TABLE I. - DOOR HINGE LOCATION

Door position	Upstream door				Downstream door			
	Length, L_{δ_1}		Diameter, d_{δ_1}		Length, L_{δ_2}		Diameter, d_{δ_2}	
	in.	cm	in.	cm	in.	cm	in.	cm
10°-20°	2.396	6.085	8.26	20.98	7.48	18.99	4.25	10.79
8°-16°	2.447	6.215	8.23	20.90	7.54	19.14	4.28	10.86
5°-10°	2.553	6.485	8.13	20.64	7.82	19.85	4.32	10.96
20°	3.293	8.365	7.85	19.94	----	-----	----	-----
16°	3.293	8.365	7.85	19.94	----	-----	----	-----
10°	3.293	8.365	7.85	19.94	----	-----	----	-----
Closed[a]	-----	-----	----	-----	----	-----	----	-----

[a]Hinge location simulated each door position.

TABLE II. - DOOR STATIC-PRESSURE ORIFICE LOCATIONS

Door position	Internal, $\theta = 0^{\circ}$			External, $\theta = 167.5^{\circ}$		
	Tap	Axial distance, x		Tap	Axial distance, x	
		in.	cm		in.	cm
10°-20°	1	-6.77	-17.20	1	-7.19	-18.26
	2	-6.04	-15.34	2	-6.69	-17.00
	3	-5.44	-13.81	3	-6.04	-15.34
	4	-4.70	-11.94	4	-5.35	-13.59
	5	-3.87	-9.83	5	-4.71	-11.97
	6	-3.27	-8.30	6	-4.10	-10.42
				7	-3.43	-8.72
8°-16°	1	-6.81	-17.29	1	-7.16	-18.18
	2	-6.12	-15.54	2	-6.68	-16.98
	3	-5.46	-13.86	3	-6.02	-15.30
	4	-4.48	-11.39	4	-5.34	-13.56
	5	-3.64	-9.25	5	-4.68	-11.90
	6	-3.26	-8.27	6	-3.99	-10.14
				7	-3.38	-8.58
5°-10°	1	-6.60	-16.75	1	-7.08	-17.99
	2	-6.02	-15.30	2	-6.68	-16.98
	3	-5.41	-13.73	3	-6.00	-15.25
	4	-4.70	-11.93	4	-5.33	-13.54
	5	-4.00	-10.16	5	-4.66	-11.83
	6	-3.32	-8.42	6	-3.99	-10.14
				7	-3.32	-8.42
20°	1	-5.97	-15.17	1	-6.30	-16.00
	2	-5.39	-13.70	2	-5.75	-14.60
	3	-4.65	-11.82	3	-5.31	-13.49
	4	-4.08	-10.35	4	-4.86	-12.34
	5	-3.66	-9.31	5	-4.39	-11.14
	6	-3.27	-8.30	6	-4.08	-10.37
				7	-3.36	-8.53
16°	1	-6.00	-15.25	1	-6.17	-15.67
	2	-5.44	-13.81	2	-5.75	-14.61
	3	-4.79	-12.17	3	-5.29	-13.44
	4	-4.15	-10.53	4	-4.82	-12.25
	5	-3.68	-9.34	5	-4.34	-11.01
	6	-3.25	-8.26	6	-3.83	-9.72
				7	-3.30	-8.38
10°	1	-6.13	-15.57	1	-7.54	-19.16
	2	-5.49	-13.94	2	-5.76	-14.62
	3	-4.92	-12.51	3	-5.27	-13.39
	4	-4.37	-11.09	4	-4.78	-12.14
	5	-3.81	-9.67	5	-4.28	-10.87
	6	-3.25	-8.26	6	-3.76	-9.56
				7	-3.24	-8.22
Closed	1	-7.36	-18.70	1	-7.54	-19.16
	2	-6.09	-15.47	2	-7.29	-18.51
	3	-5.13	-13.03	3	-3.52	-8.94
	4	-3.11	-7.90			

TABLE III. - TOTAL-PRESSURE PROBE LOCATIONS

(a) Open- and closed-door total-pressure rake. Open-door rake at model station 133.86 inches (340 cm); circumferential location, $\theta = 112.5^{\circ}$; door 6. Closed-door rake at model station 123.62 inches (314 cm); circumferential location, $\theta = 135^{\circ}$; door 7

Probe	Radial distance from secondary shroud external surface, z	
	in.	cm
1	0.125	0.318
2	.500	1.270
3	1.000	2.540
4	1.800	4.572
5	2.750	6.985

(b) Auxiliary inlet total-pressure rake. Circumferential position, $\theta = 225^{\circ}$; door 11

Probe	Radial distance from secondary shroud internal surface, z'	
	in.	cm
1	0.062	0.158
2	.312	.792
3	.500	1.270
4	.750	1.905
5	1.000	2.540

(c) Primary nozzle secondary total-pressure probes

Probe	Radius, r		Circumferential location, θ, deg
	in.	cm	
1	3.25	8.26	0
2	↓	↓	90
3			180
4			270

Nozzle Instrumentation

An internal row of static-pressure orifices was located on door 1 (fig. 4(b)), at a meridian angle of 0° and externally on door 8 at a meridian angle of 167.5°. The door hinge location is given in table I, and the axial locations x of the door static-pressure orifices are given in table II. The hinge moment analysis for the auxiliary inlet doors is given in appendix C.

The primary, secondary, boundary-layer, and tertiary total pressures were obtained from total-pressure probes located as shown in figures 5(a) and (b). When the doors were closed, the boundary-layer rake was located upstream of the doors at 135°. Table III gives the radial location of the secondary, door, and auxiliary inlet total-pressure probes. The radial location of the primary rake probes are given in figure 5(b). A row of static-pressure orifices was located at a meridian angle of 90° on the flap internal surface and 180° along the external boattail. The axial locations x of the static-pressure orifices are given in table IV.

Primary total-pressure profiles of the internal flow entering the primary nozzle are shown in figure 6. The nozzle inlet total pressure P_7 was obtained by integrating the pressure across an area-weighted rake located in the primary flow passage at station 7 and dividing by the total cross-sectional area. The flow was assumed to be circumferentially uniform.

TABLE IV. - SECONDARY SHROUD STATIC-PRESSURE ORIFICE LOCATIONS

Internal, $\theta = 90^{\circ}$			External, $\theta = 180^{\circ}$		
Tap	Axial distance, x		Tap	Axial distance, x	
	in.	cm		in.	cm
1	-1.811	-4.60	1	-1.370	-3.48
2	-1.146	-2.91	2	1.925	4.89
3	-.396	-1.006	3	2.661	6.76
4	.614	1.56	4	3.142	7.98
5	1.811	4.60	5	3.535	8.98
6	2.669	6.78	6	3.949	10.03
7	3.402	8.64	7	4.362	11.08
8	4.158	10.56	8	4.787	12.16
9	4.925	12.51	9	5.232	13.29
10	5.705	14.49	10	5.689	14.45
11	6.512	16.54	11	6.165	15.66
			12	6.658	16.91

Procedure

The turbojet nozzle pressure ratio schedule shown in figure 7 was used as a guide for setting the nozzle pressure ratio over the range of Mach numbers from 0 to 1.20 for each power setting. This schedule is typical for an afterburning turbojet engine that is applicable to a supersonic-cruise aircraft. At each Mach number, data were taken at several nozzle pressure ratios around the values shown in figure 7. The nozzle pressure ratio was varied by changing the nozzle inlet pressure. The maximum pressure ratio at each Mach number was restricted because of the limitations of the primary air supply and the ambient pressure at that Mach number. Corrected secondary weight flow was varied from 0 to 16 percent of the primary flow. The general nozzle performance characteristics are presented in appendix B. Results presented and discussed in the following section are only for the pressure ratio schedule shown in figure 7.

RESULTS AND DISCUSSION

Comparison of Single- and Double-Hinge Inlet Door Performance

A comparison of the best-measured nozzle efficiencies of the single- and double-hinge doors over a range of free-stream Mach number at two simulated power settings is shown in figure 8. The term "best-measured nozzle efficiency" is used to indicate the highest nozzle efficiency obtained for the specific door configurations tested at each Mach number. However, untested door positions may have provided higher nozzle efficiencies. A 4-percent corrected secondary-weight-flow ratio was chosen as being typical for these two power settings. For dry acceleration, the single-hinge door configuration had a slightly higher nozzle efficiency than the double-hinge doors. At takeoff, the single-hinge configuration had a nozzle efficiency of 0.990 compared to 0.982 with the double-hinge configuration. At Mach 0.90, the single- and double-hinge door configurations both had a peak nozzle efficiency of approximately 0.920. The results obtained at subsonic cruise (fig. 8) indicate that a double-hinge door configuration provided better nozzle efficiency especially at Mach 0.70. At Mach 0.90, the nozzle efficiencies for the single- and double-hinge door configurations were 0.891 and 0.897, respectively. No data are shown in figure 8 for the reheat power setting beyond takeoff because the doors generally would be closed.

Typical curves of the boattail drag to ideal gross-thrust ratio are presented in figure 9 for three power settings. In general, the boattail drag was independent of both the door type (single or double hinge) and position in the region where best measured and estimated floating nozzle efficiencies occurred. An explanation of how the estimated

floating performance was obtained is given in appendix C. The boattail drag varied from 1 percent of the ideal gross thrust at Mach 0.70 to about 9 percent at Mach 1.00 for the subsonic-cruise power setting. However, with the larger ideal gross thrust obtained at the higher nozzle pressure ratio (dry acceleration), the boattail drag was a smaller percentage of the ideal gross thrust, varying from 1/2 percent at Mach 0.70 to 5 percent at Mach 1.00. With reheat, the boattail drag was unimportant at Mach numbers up to 0.85 and had a maximum value of about 3 percent of the ideal gross thrust at Mach 1.20.

Single-Hinge Inlet Door Performance

The performance and secondary total-pressure recovery requirements of the single-hinge inlet door configurations are shown in figure 10 as a comparison between the estimated floating position performance and the best measured performance. The data points representing the estimated floating performance are obtained from crossplots. Figure 10(a) shows that there was little difference between best measured and estimated floating door nozzle efficiency up to Mach 0.95 at the subsonic-cruise power setting. The best measured nozzle efficiency was obtained with the 16° door configuration. At Mach 0.70, the 16° door position was about the same as the floating-door equilibrium position. At higher speeds, the equilibrium door position was less than that required for best measured nozzle efficiency. At the subsonic-cruise Mach number (0.90), nozzle efficiencies of 0.891 and 0.885 were obtained at the best measured (16°) and estimated floating (10°) positions, respectively. Pumping characteristics were adequate to provide 4-percent corrected secondary weight flow from a free-stream source at the subsonic-cruise power setting. At both subsonic-cruise and dry-acceleration power settings (figs. 10(a) and (b)), the required secondary total-pressure recovery was increased significantly by opening the doors from the estimated floating position. This increased secondary total pressure is indicative of an increased pressure level in the primary base region which, in turn, was responsible for the small increased performance. A curve of free-stream static-pressure ratio is presented in figures 10(a) and (b) for comparison. By forcing the doors to remain open, secondary total pressures considerably above p_0 were obtained. These higher pressures were also responsible for forcing the floating doors to partly close. At the dry-acceleration power setting (fig. 10(b)), the best measured nozzle efficiency was moderately higher than the estimated floating efficiency. The largest difference occurred at takeoff and at Mach 1.00 where the peak performance was about 2.5 percent higher than that obtained from the equilibrium door position. At takeoff, the best measured nozzle efficiency was 0.99 compared to 0.967 for the estimated floating efficiency. The door position for best measured nozzle efficiency was 16° from takeoff to Mach 0.85 and 10° from Mach 0.90 to 1.00. Floating-door angles

were always lower than those required for peak nozzle efficiency. It would be difficult to supply 4-percent corrected secondary weight flow from a free-stream source at take-off. However, from Mach 0.60 to 1.00 the pumping characteristics were such that 4-percent corrected secondary weight flow could be provided from a free-stream source. For reheat acceleration (fig. 10(c)), the peak measured performance was obtained with the inlets closed at Mach numbers greater than 0.60. The inlet door moments also indicated that the doors should be closed at Mach numbers of 0.85 to 1.20. However, the 4-percent corrected secondary weight flow assumed to be needed to cool the nozzle could not be obtained from a free-stream source with the flap in the position tested. The relatively poor performance obtained at the reheat power setting is due, in part, to the fixed-converging single-hinge trailing-edge flap. The trailing-edge flap moments indicated that the flaps (if aerodynamically positioned) would float out and probably result in a performance improvement (in both nozzle efficiency and pumping characteristics).

The effect of the single-hinge inlet door angle on nozzle efficiency is shown in figure 11 for three power settings at assumed trajectory conditions. As pointed out previously, the 16° door configuration had the best measured nozzle efficiency at subsonic cruise and dry acceleration (figs. 11(a) and (b)). The difference between the open and solid symbols in figure 11(b) with the inlet doors closed indicated that the nozzle efficiency was very sensitive to small changes in nozzle pressure ratio (0.2 to 1 percent) near the trajectory value. This phenomenon is discussed further in connection with figure 16. However, at these conditions the inlet doors would generally be open. In the reheat acceleration range (fig. 11(c)), the nozzle was fully expanded at Mach 1.00 and above. Therefore, the closed-door configuration provided the best measured nozzle efficiency.

Pressure forces were calculated at Mach 0.90 on the inlet doors and the secondary shroud for the three power settings. These component forces were computed over a range of inlet door angles and are presented in figure 12 as a ratio to the combined ideal primary and secondary thrust. The secondary momentum was calculated by assuming a constant static pressure between the primary nozzle and the internal door surface. When the doors were open, several of the internal forces changed sign at the subsonic-cruise power setting (fig. 12(a)). At this flight condition, floating doors would be open at an angle of about 10°. The largest drag force was measured externally on the trailing-edge flap section. Internally on the shroud and flap, the two components partially cancel each other to provide a net drag of a little over 1 percent of the ideal thrust. However, at dry and reheat acceleration (figs. 12(b) and (c), respectively), a large drag force occurred on the upstream surface of the secondary shroud, in addition to the boattail drag.

A simple pin connection was assumed in calculating the moments on the single-hinge doors (fig. 13). Door equilibrium is defined in appendix C. In general, a double equi-

librium position existed at subsonic cruise and during dry-acceleration power settings over the Mach number range tested (figs. 13(a) and (b)). Hence, the following hypothesis was made: the tendency of the doors, if free floating, would be to close as the free-stream Mach number is increased for a given flight pressure ratio schedule. The foregoing hypothesis eliminates the equilibrium position between the 16° and 20° door. There is, however, a large range over which the moment is rather small, allowing the door position to be easily affected by other flows or forces. The doors would be open at the subsonic-cruise and dry-acceleration power settings but closed with reheat above Mach 0.7 (fig. 13(c)).

Internal and external static-pressure distributions on the inlet doors and the secondary shroud upstream surface are shown in figure 14 at Mach 0.90 for subsonic cruise and dry acceleration and at Mach 0 and 0.95 for reheat acceleration. At subsonic cruise (fig. 14(a)), the nozzle was overexpanded internally with the doors closed. However, the overexpansion was generally eliminated when the tertiary inlets were open. At the higher pressure ratio for dry acceleration (fig. 14(b)), opening the doors increased the internal nozzle pressure upstream of the secondary shroud throat to values 15 percent larger than free-stream static. This is indicative of the significant diffusion of the incoming tertiary flow as it enters the nozzle. For a reheat takeoff (fig. 14(c)), opening the inlet doors caused a slight increase in both internal pressures and nozzle efficiency. The doors should be fully open at reheat takeoff for best nozzle efficiency. However, for a reheat acceleration at Mach 0.95 (fig. 14(d)), opening the inlet doors caused a reduction in the internal pressures and a loss in nozzle efficiency. The doors should be closed at this flight condition for best efficiency.

Figure 15 shows the effect of door position on the inlet door velocity profiles at subsonic cruise and dry acceleration. The peak velocity occurred along the secondary flap internal leading edge (opposite the external door surface). At subsonic cruise, the peak velocities were generally between 70 and 80 percent of the free-stream velocity. The tertiary flow was reduced at Mach 0.95 and 1.00 with the 16° doors (fig. 15(a)). The peak inlet velocities were reduced at the higher nozzle pressure ratios required for dry acceleration (fig. 15(b)). There was even evidence of separated flow for the 16° door position at Mach numbers from 0.85 to 1.00 and for all three door positions at Mach 1.00. At these conditions, floating doors would generally be at angles less than 10° or completely closed. Separated flow was generally observed during reheat acceleration, but these data are not presented since the doors should be closed under those conditions.

The effect of single-hinge inlet door position on the trailing-edge flap moment coefficient per inch of width is presented in figure 16 for the three power settings. The trailing-edge flaps, if floating, would be off the inner stop at subsonic cruise and during reheat acceleration. At these conditions, in general, the moment coefficient per inch of width is independent of door position. From takeoff to Mach 0.95 the trailing-edge flaps

would be on the inner stop during a dry acceleration when the inlet doors are open. However, with the doors closed, the flap moment was very sensitive to a small change in pressure ratio for the dry-acceleration configuration, as mentioned earlier and shown in figure 11(b). This phenomenon results in a double-value flap moment as shown in figure 16(b).

Static-pressure distribution through the secondary shroud is shown during dry acceleration with the inlet doors closed in figure 17. At Mach numbers from 0.60 to 1.00, a slight change in nozzle pressure ratio (at the trajectory value) resulted in a large change in pressure distribution on the internal surface of the trailing-edge flap aft of the hinge point. At the lower nozzle pressure ratio, internal flap pressures recovered to values greater than free-stream static pressure and equal to about 33 percent of P_7. At the higher nozzle pressure ratio, the flow appeared to go through an oblique shock at the hinge point and then accelerate downstream. This provided higher nozzle efficiency, as shown previously in figure 11(b). Trailing-edge flap moments also changed sign as shown in figure 16(b). Floating flaps might become unstable at these flight conditions.

Double-Hinge Inlet Door Performance

The performance characteristics of the double-hinge inlet doors are presented in figures 18 to 24. In general, the effect of inlet door angle on performance, door moments, inlet velocity profiles, and flap moment was similar to that obtained with the single-hinge doors as discussed in the preceding section. A comparison between the estimated floating and best measured nozzle efficiencies (figs. 18(a) and (b)) indicates that, in general, the efficiency for the floating door position is lower at both subsonic-cruise and dry-acceleration power settings. For example, at Mach 0.90 (subsonic cruise, fig. 18(a)), the best measured nozzle efficiency is 0.897, compared to 0.885 for the estimated floating efficiency. At the higher nozzle pressure ratios for dry acceleration (fig. 18(b)), the efficiencies at Mach 0.90 are 0.921 and 0.907 for the peak and estimated floating positions, respectively. The floating door angle was always less than that required for best measured nozzle efficiency. Corrected secondary-weight-flow ratios of 4 percent could be provided from a free-stream source at Mach numbers from 0.70 to 1.00 with both subsonic-cruise and dry-acceleration power settings (figs. 18(a) and (b)). Opening the doors again forced the secondary total-pressure requirements to be in excess of free-stream static, which is indicative of the doors' ability to raise internal pressures above p_0. With reheat acceleration (fig. 18(c)), the closed-door configuration produced the highest performance. The secondary total-pressure recovery characteristics indicate that corrected secondary-weight-flow ratios of 4 percent could not be provided from a free-stream source at takeoff with either a dry or a reheat power setting. However, at takeoff with reheat, the shroud wants to open; permitting it to do

so could result in a reduction in the secondary total-pressure recovery. This condition also existed at Mach numbers from 0.85 to 1.20 for the reheat-acceleration configuration (fig. 18(c)).

The effect of double-hinge inlet door angle on nozzle efficiency is presented in figure 19 for the three power settings. Data are presented at several Mach numbers at the trajectory pressure ratios. At subsonic cruise and dry acceleration (figs. 19(a) and (b)), opening the inlet doors to 8°-16° generally produced the optimum nozzle efficiency. At the dry-acceleration power setting (fig. 19(b)), the nozzle efficiency was very sensitive to the nozzle pressure ratio at Mach numbers above takeoff. For a reheat acceleration, the fully expanded nozzle pressure ratio is 5.65. Figure 19(c) shows that the closed-door configuration produced the optimum nozzle efficiency at Mach numbers of 0.60 and higher where the nozzle pressure ratio approached the fully expanded value. For this configuration, a slightly higher nozzle efficiency was obtained with the inlet doors open at takeoff.

Pressure forces were calculated for the three power settings at Mach 0.90 on the double-hinge inlet doors and the secondary shroud. These forces were calculated over a range of door angles and are presented in figure 20 as a ratio to the combined ideal primary and secondary thrust. The secondary momentum was calculated by assuming a constant static pressure between the primary nozzle and the internal door surface. All the internal secondary shroud forces changed sign from closed to open inlet doors at the subsonic-cruise power setting (fig. 20(a)). Drag forces were measured on both the internal and external surfaces of the trailing-edge flap with open inlet doors. Thrust and drag on the diverging and contracting portions of the shroud combine to provide a net drag of about 1 percent. High pressure in the inlet door region produced thrust on the rear door segment and drag on the upstream shroud surface. At dry and reheat acceleration (figs. 20(b) and (c)), a large drag force existed on the upstream shroud surface that forms part of the inlet system. However, a small net thrust was measured on the double-hinge inlet door. The shroud as a whole sustained a large net drag.

The method used to calculate hinge moments for the double-hinge door configurations is described in appendix C. The moment coefficients indicate that the doors would float between 2.5°-5° and 5°-10° at subsonic cruise (fig. 21(a)). For a dry acceleration (fig. 21(b)), the doors would be fully open at takeoff, partly open at Mach numbers from 0.60 to 0.85, and closed at Mach numbers of 0.90 and above. For a reheat acceleration (fig. 21(c)), the double-hinge doors would be closed above takeoff.

Internal and external pressure distributions on the inlet doors are presented in figure 22. Data are presented at Mach 0.90 for several door angles at a subsonic-cruise pressure ratio (fig. 22(a)), and at a dry-acceleration pressure ratio (fig. 22(b)). These data show a recompression of the flow on the downstream surfaces of the inlets. For a reheat takeoff (fig. 22(c)), opening the inlet doors caused both a slight increase in inter-

nal pressures and nozzle efficiency. The doors would be fully open at this flight condition for best nozzle efficiency. However, for a reheat acceleration at Mach 0.95 (fig. 22(d)), opening the inlet doors caused a reduction in the internal pressures and a loss in nozzle efficiency. The inlet doors should be closed at this flight condition for best efficiency.

The effect of the double-hinge inlet door position on auxiliary inlet flow velocity profiles is presented in figure 23 for subsonic-cruise and dry-acceleration power settings. Peak inlet velocities were generally between 70 and 80 percent of the free-stream velocity at subsonic-cruise conditions and door angles up to 8°-16°. These velocity profiles indicate that most of the flow exists near the downstream surfaces of the auxiliary inlets. Flow separation from the doors is indicated for 10°-20° doors at Mach numbers from 0.85 to 1.00. At the higher nozzle pressure ratios required for dry acceleration (fig. 23(b)), the peak inlet velocities were reduced to between 60 and 70 percent of the free-stream velocity. The inlet flow was generally reduced at the higher Mach numbers between 0.90 and 1.00 where the moments indicated that floating doors would be closed.

The effect of double-hinge door position on the trailing-edge flap moment coefficient per inch of width is presented in figure 24 for the three power settings. If the trailing-edge flaps were allowed to float, they would be off the inner stop at subsonic cruise and maximum reheat (figs. 24(a) and (c)). At these conditions, in general, the moment coefficient per inch of width is independent of door position. At dry-acceleration power setting (fig. 24(b)), the flaps would tend to be on or near the inner stop.

Model Boundary-Layer Characteristics

The boundary-layer characteristics have been measured previously on this jet-exit model over a range of Mach number from 0.56 to 1.46 and are presented and discussed in reference 6. These measurements indicate a well-developed turbulent profile with an average momentum-thickness-to-model-diameter ratio of about 0.019 for the Mach number range of this report. A single rake measurement was made during the current test with the inlet doors closed and the resulting boundary-layer profiles are shown on figure 25 for two power settings. Also shown for the same conditions is a boundary-layer profile downstream of the 10°-20° double-hinge inlet doors. Opening the inlet doors generally reduced the local external flow velocity downstream of the doors for subsonic-cruise power settings (fig. 25(a)). For a dry acceleration (fig. 25(b)), opening the inlet doors generally increased the local external velocity downstream of the inlets, particularly at Mach numbers from 0.85 to 1.00. There was evidence of some separated inlet flow at these conditions, as mentioned previously in the discussion of figure 23(b).

SUMMARY OF RESULTS

An experimental investigation was conducted to determine the performance of an auxiliary inlet ejector nozzle at free-stream Mach numbers from 0 to 1.20. The auxiliary inlet configurations consisted of fixed-position single-hinge doors (10°, 16°, and 20°), double-hinge doors (5°-10°, 8°-16°, and 10°-20°), and a closed door, which provided variations in tertiary flow area from 0 to 71.5 percent of the shroud exit area. The shroud was comprised of a single-hinge flap which was fixed in a subsonic-cruise position. Its projected boattail area was 47 percent of the simulated nacelle area. Two different primary throat areas were used: one to simulate nonreheat operation (subsonic cruise and dry acceleration) and the other for reheat operation. The following results were obtained at three indicated flight conditions based on a pressure ratio schedule appropriate for an afterburning turbojet engine and a corrected secondary-weight-flow ratio of 4 percent:

Subsonic cruise:

1. The double-hinge doors provided higher nozzle efficiency than the single-hinge doors below Mach 1.00. The performance difference varied from 3 percent at Mach 0.70 to a negligible difference at Mach 1.00.

2. The estimated floating door angle was generally less than that required for best measured nozzle efficiency. However, the estimated floating performance was near the best measured value.

3. Pumping characteristics were adequate to provide 4-percent corrected secondary flow from a free-stream source.

4. For the best measured performance, boattail drag varied from 1 percent of the ideal gross thrust at Mach 0.70 to 9 percent at Mach 1.00.

5. Trailing-edge flap moment coefficients indicated an opening moment for the fixed position tested. Flap position might influence floating door position and nozzle efficiency.

6. Peak inlet velocities were generally between 70 and 80 percent of free-stream velocity. The tertiary inlet flow generally reduced the local free-stream velocity measured downstream of the auxiliary inlets.

7. In general, opening the doors increased the internal door pressures to, or above, free-stream static pressure.

Dry acceleration:

1. The single-hinge doors provided slightly better measured nozzle efficiency at subsonic speeds.

2. The estimated floating-door angle was generally less than that required for best measured nozzle efficiency, although the estimated floating performance was near the best measured value.

3. Pumping characteristics were adequate to provide 4-percent corrected secondary flow from a free-stream source at all Mach numbers except takeoff.

4. Boattail drag varied from 1/2 percent of the ideal gross thrust at Mach 0.70 to 5 percent at Mach 1.00.

5. At Mach 0.60 and above, the trailing-edge flap moment coefficients indicated a closing moment for the fixed position tested.

6. Peak inlet velocities were generally between 60 and 70 percent of free-stream velocity. Separated flow was measured for some door positions at Mach numbers of 0.85 and greater.

7. Opening the inlet doors generally increased the internal door pressures above p_0.

Reheat acceleration:

1. At Mach 0.60 and higher, the best measured nozzle efficiency was obtained with the doors closed.

2. Trailing-edge flap moment coefficients indicated an opening moment for the fixed position tested at all Mach numbers.

3. Pumping characteristics were inadequate at all Mach numbers to supply 4-percent corrected secondary flow from a free-stream source.

4. Boattail drag was unimportant at Mach numbers to 0.85 and had a value of 3 percent of the ideal gross thrust at Mach 1.20.

Lewis Research Center,
National Aeronautics and Space Administration,
Cleveland, Ohio, February 11, 1970,
126-15.

APPENDIX A

SYMBOLS

A	area (projected)
A_{max}	simulated nacelle area
AR	aspect ratio (width/length)
A_{ter}	tertiary flow area normal to external door tip
C_{D8}	nozzle flow coefficient, w_p/w_i
C_m	moment coefficient, $\frac{\sum m_{ext} - \sum m_{int}}{(A_{max})(d_{max})(P_7)}$
D	drag
d	diameter
d_{max}	model diameter (equivalent to the simulated nacelle diameter)
d_s	minimum diameter of secondary shroud
F	thrust
$F_1, \ldots, F_4$	forces acting on door
L	length
l	length of secondary shroud, 9.842 in. (25.0 cm)
M	Mach number
m	moment
P	total pressure
p	static pressure
R	total radius
r	radius from centerline to local probe
s	axial distance from primary nozzle exit to minimum secondary shroud diameter
T	total temperature
V	velocity
w	weight-flow rate

x	axial distance measured from secondary shroud minimum diameter
z	radial distance from secondary shroud external surface
z'	radial distance from secondary shroud internal surface
α	primary nozzle flap angle
β	boattail angle
δ	door angle
θ	circumferential position, deg
$\varphi_2, \varphi_3, \varphi_5$	force angle (double-hinge door moment analysis)
$\omega\sqrt{\tau}$	corrected secondary-weight-flow-rate ratio, $(w_s/w_p)\sqrt{T_s/T_p}$

Subscripts:

d	door
ext	external
f	flap
i	ideal
int	internal
p	primary
s	secondary
ter	tertiary
x	condition at distance x
0	free stream
1	upstream door
2	downstream door
7	nozzle inlet
8	nozzle throat
9	nozzle exit

APPENDIX B

NOZZLE PERFORMANCE CHARACTERISTICS

Nozzle gross-thrust coefficients and pumping characteristics obtained during testing are presented for each auxiliary inlet door configuration: first, for primary nozzle configuration I ($A_9/A_8 = 1.99$); and then for primary nozzle configuration II ($A_9/A_8 = 1.42$). Data are presented as a function of nozzle pressure ratio and corrected secondary-weight-flow ratio for a range of Mach number (figs. 26 to 29).

APPENDIX C

AUXILIARY INLET DOOR HINGE MOMENT ANALYSIS

For single-hinge doors, the hinge moment was obtained simply by integrating the moments of the internal and external pressure distributions. To obtain the hinge moment about the front hinge of a double-hinge door, the fixed door was assumed to have the mechanism shown in figure 30. This mechanism, with $l_4 = 2l_6$ would give a door angle ratio δ_2/δ_1 of approximately 2.0.

The equations to determine the total hinge moment at Z are as follows: Considering the rear door as a free body in equilibrium, the sum of the forces and moments about X would be equal to zero.

$$F_1 l_1 - F_2 l_2 = 0 \tag{C1}$$

$$F_1 \sin \delta_2 + F_2 \sin \varphi_2 - F_3 \sin \varphi_3 = 0 \tag{C2}$$

$$F_1 \cos \delta_2 + F_2 \cos \varphi_2 - F_3 \cos \varphi_3 = 0 \tag{C3}$$

In these equations, F_3 is considered as the equilibrant; δ_2, φ_2, and l_2 are known constants for any particular door setting; F_1 and l_1 are determined from the measured pressure distribution on the rear door; F_2 is the reaction of the pin Y against the side of the slot and must be normal to the side of slot; F_2, φ_3, and F_3 can be determined from the solution of equation (C1) and the simultaneous solution of equations (C2) and (C3).

$$F_2 = \frac{F_1 l_1}{l_2} \tag{C4}$$

$$\varphi_3 = \tan^{-1} \frac{F_1 \sin \delta_2 + F_2 \sin \varphi_2}{F_1 \cos \delta_2 + F_2 \cos \varphi_2} \tag{C5}$$

$$F_3 = \frac{F_1 \sin \delta_2 + F_2 \sin \varphi_2}{\sin \varphi_3} \tag{C6}$$

Then the moment about Z caused by the forces on the rear door is

$$m_{F\text{-}R} = F_3 l_3 = F_3 l_4 \cos \varphi_3 = F_3 l_4 \cos(\varphi_3 - \delta_1) \tag{C7}$$

where F_3 is the resultant of F_1 and F_2, and δ_1 and l_4 are known constants for any particular door setting. The total moment about Z is then

$$m_Z = m_{F\text{-}R} + F_4 l_5 \tag{C8}$$

where F_4 and l_5 are obtained from the measured internal and external pressure distributions on the front door.

For both single- and double-hinge door configurations, door equilibrium is defined as (1) that angle where the moment curve passes through zero moment with a negative slope, or (2) the condition where moments on the closed doors are negative ($p_{int} > p_{ext}$). At the latter condition, the doors are on the "outer stop" and, hence, in equilibrium.

REFERENCES

1. Steffen, Fred W.; and Jones, John R.: Performance of a Wind Tunnel Model of an Aerodynamically Positioned Variable Flap Ejector at Mach Numbers From 0 to 2.0. NASA TM X-1639, 1968.

2. Bresnahan, Donald L.: Experimental Investigation of a 10^{o} Conical Turbojet Plug Nozzle With Iris Primary and Translating Shroud at Mach Numbers From 0 to 2.0. NASA TM X-1709, 1968.

3. Shrewsbury, George D.; and Jones, John R.: Static Performance of an Auxiliary Inlet Ejector Nozzle for Supersonic-Cruise Aircraft. NASA TM X-1653, 1968.

4. Blaha, Bernard J.; and Bresnahan, Donald L.: Wind Tunnel Installation Effects on Isolated Afterbodies at Mach Numbers From 0.56 to 1.5. NASA TM X-52581, 1969.

5. Smith, K. G.: Methods and Charts for Estimating Skin Friction Drag in Wind Tunnel Tests With Zero Heat Transfer. Rep. ARC-CP-824, Aeronautical Research Council, Great Britain, 1965.

6. Harrington, Douglas E.: Jet Effects on Boattail Pressure Drag of Isolated Ejector Nozzles at Mach Numbers From 0.60 to 1.47. NASA TM X-1785, 1969.

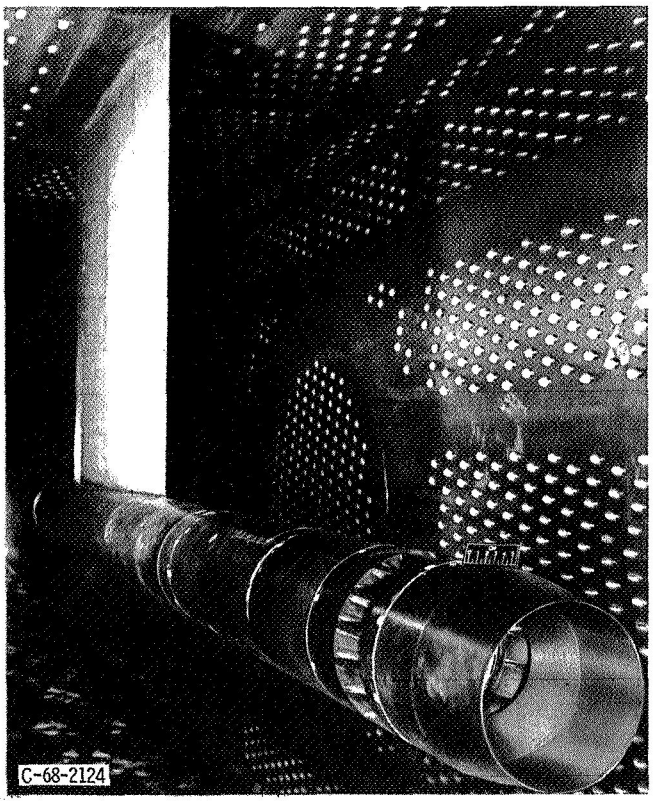

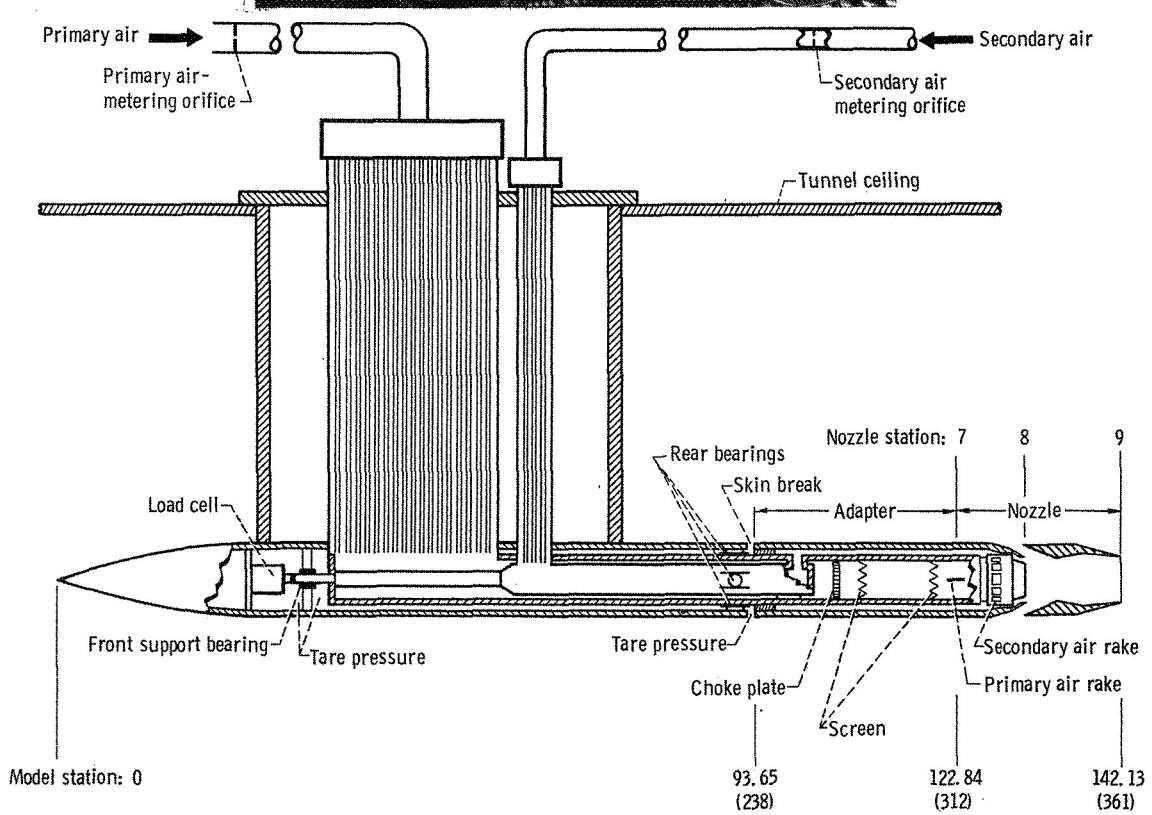

CD-10690-28

Figure 1. - Nozzle support model and thrust measuring system. (Dimensions are in inches (cm).)

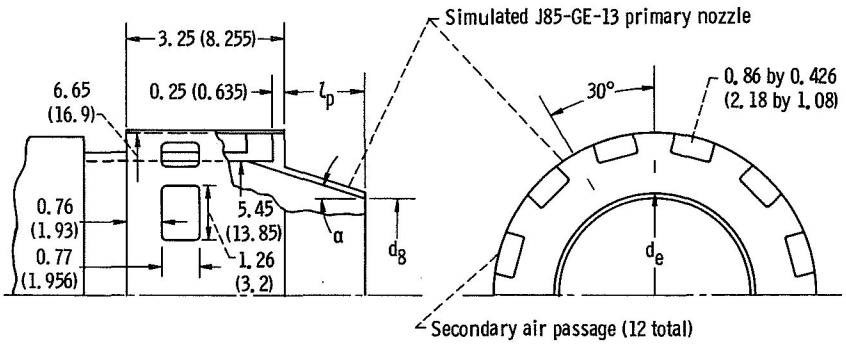

Primary nozzle configuration	Primary nozzle length, l_p		Primary nozzle diameter, d_8		Primary nozzle flap angle, α, deg	Flow coefficient, C_{D8}	External diameter of primary nozzle lip, d_e	
	in.	cm	in.	cm			in.	cm
I - Subsonic cruise and dry acceleration	1.50	3.810	4.388	11.146	13.25	0.977	4.622	11.74
II - Maximum reheat acceleration	1.08	2.743	5.192	13.188	5.30	0.985	5.437	13.81

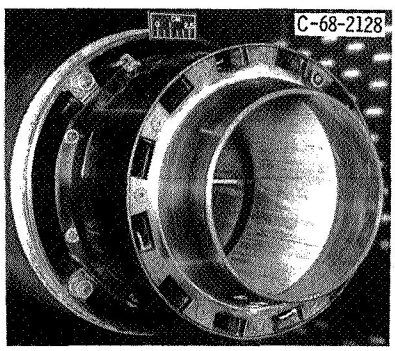

Figure 2. - Details of simulated J85-GE-13 primary nozzle. (Dimensions are in inches (cm).)

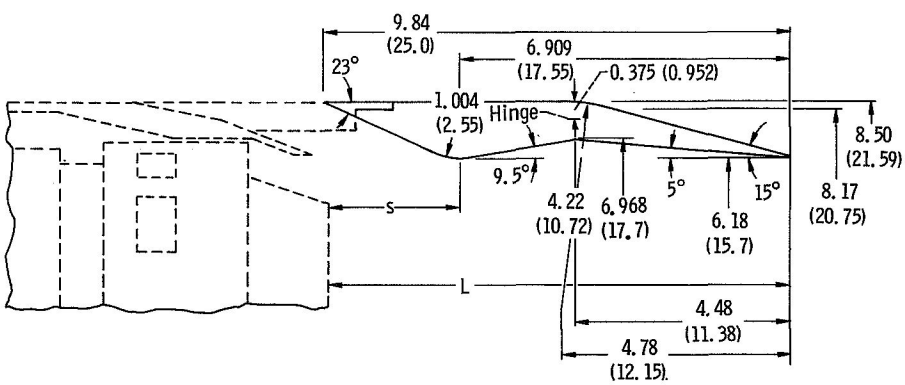

Primary nozzle configuration	Internal area ratio, A_9/A_8	Spacing ratio, s/d_8	Throat diameter ratio, d_s/d_8	Flap length ratio, L/d_8	L		s	
					in.	cm	in.	cm
I - Subsonic cruise and dry acceleration	1.99	0.585	1.408	2.16	9.477	24.07	2.566	6.52
II - Reheat acceleration	1.42	0.575	1.190	1.91	9.897	25.14	2.986	7.58

Figure 3. - Details of single-hinge trailing-edge flap. Ratio of boattail area to simulated nacelle area, $A_\beta/A_{max} = 0.47$. (Dimensions are in inches (cm).)

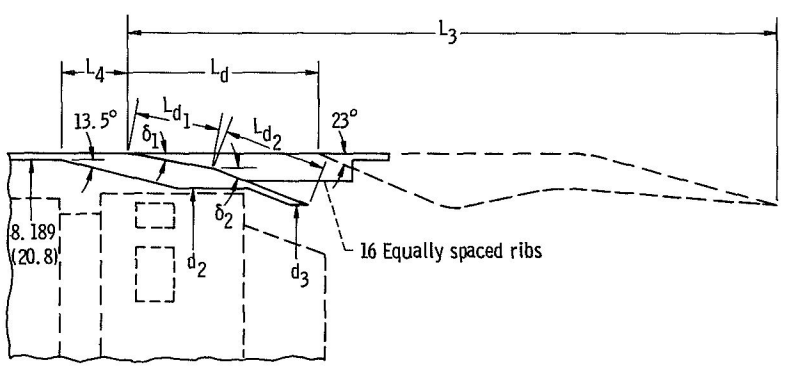

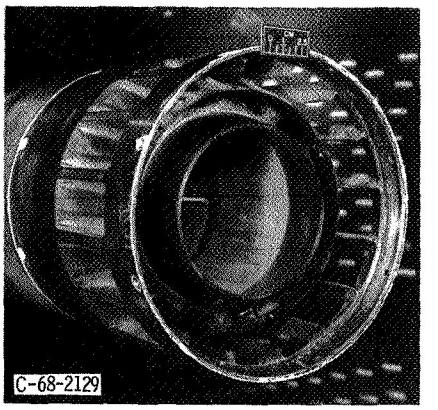

Door configuration	δ_1	δ_2	L_d		d_2		d_3		L_3		Aspect ratio, AR_d	Ratio of tertiary flow area to shroud exit area, A_{ter}/A_9	L_4		L_{d_1}		L_{d_2}	
			in.	cm	in.	cm	in.	cm	in.	cm			in.	cm	in.	cm	in.	cm
Double	10°	20°	3.972	10.09	7.0	17.78	6.386	16.22	13.78	35.00	0.306	0.715	1.369	3.48	1.895	4.81	2.040	5.13
	8°	16°	3.961	10.06	7.0	17.78	6.81	17.30	13.744	34.91	.305	.584	1.405	3.57	1.860	4.72	2.040	5.13
	5°	10°	3.854	9.79	7.441	18.90	7.441	18.90	13.634	34.63	.297	.368	1.513	3.84	1.753	4.45	2.040	5.13
Single	20°	---	3.035	7.71	7.0	17.78	6.386	16.22	12.819	32.56	0.234	0.715	2.330	5.92	3.003	7.63	-----	----
	16°	---	3.024	7.68	7.0	17.78	6.81	17.30	12.803	32.52	.233	.584	2.345	5.96	2.978	7.56	-----	----
	10°	---	2.972	7.55	7.441	18.9	7.441	18.9	12.752	32.39	.229	.368	2.392	6.08	2.919	7.41	-----	----
Closed	---	---	2.968	7.54	8.189	20.8	8.189	20.8	-----	-----	----	-----	-----	----	-----	----	-----	----

(a) Details of auxiliary inlets. (Dimensions are in inches (cm).)

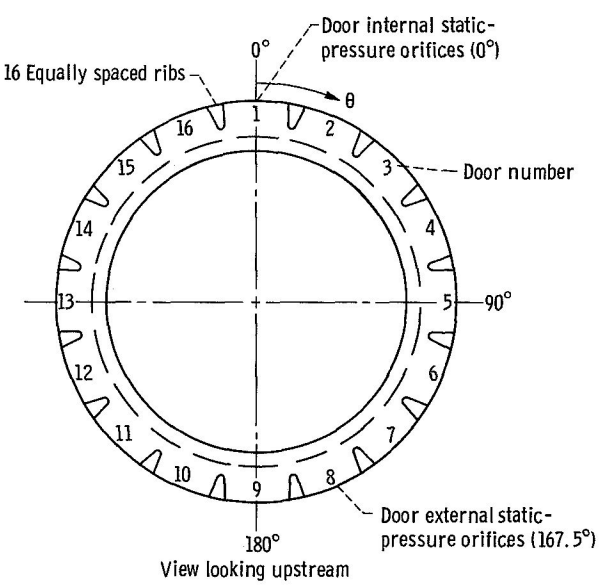

(b) End view of auxiliary inlets.

Figure 4. - Auxiliary inlets.

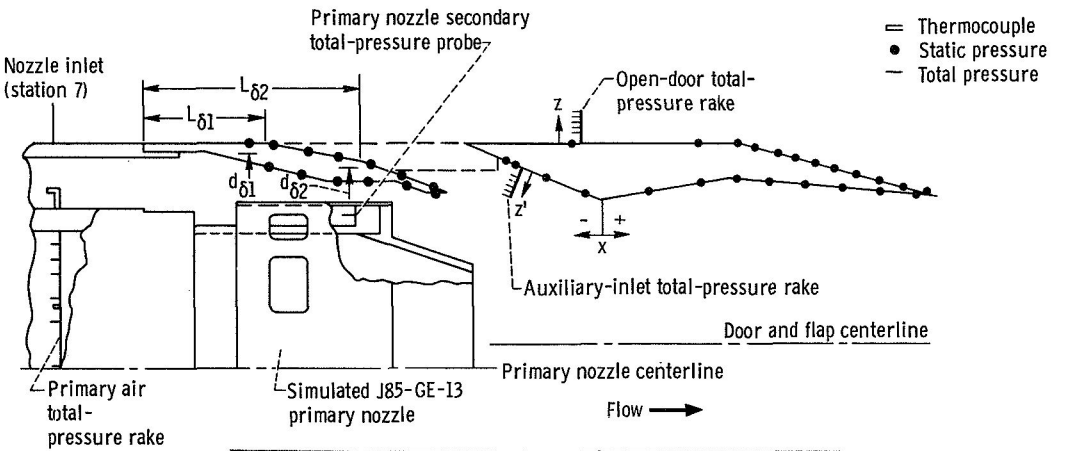

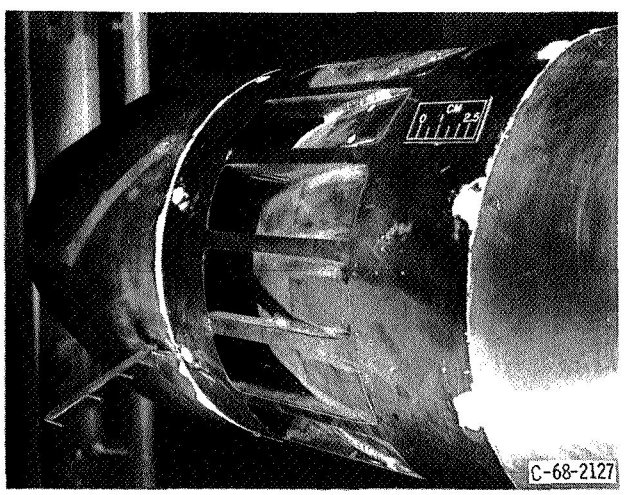

(a) Instrumentation layout.

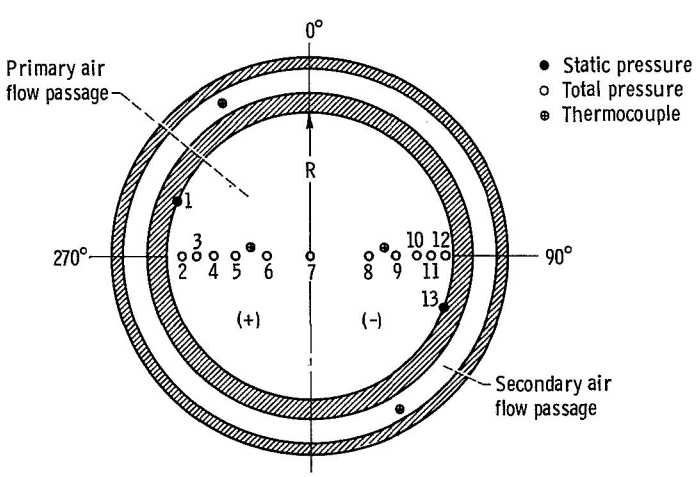

Primary flow orifice number	Normalized distance from centerline, r/R
1	1.00
2	.90
3	.790
4	.670
5	.519
6	.300
7	0
8	-.418
9	-.600
10	-.750
11	-.855
12	-.950
13	-1.00

(b) Details of instrumentation at station 7 (view looking downstream). Radius, R = 3.006 inches (7.635 cm); r is radius from center to local probe.

Figure 5. - Auxiliary inlet ejector nozzle instrumentation. See figure 5(b) for details of instrumentation at station 7. See table III for locations of total-pressure probes. See table II for door static-pressure orifice locations. See table IV for trailing-flap static-pressure orifice locations. See table I for door hinge location.

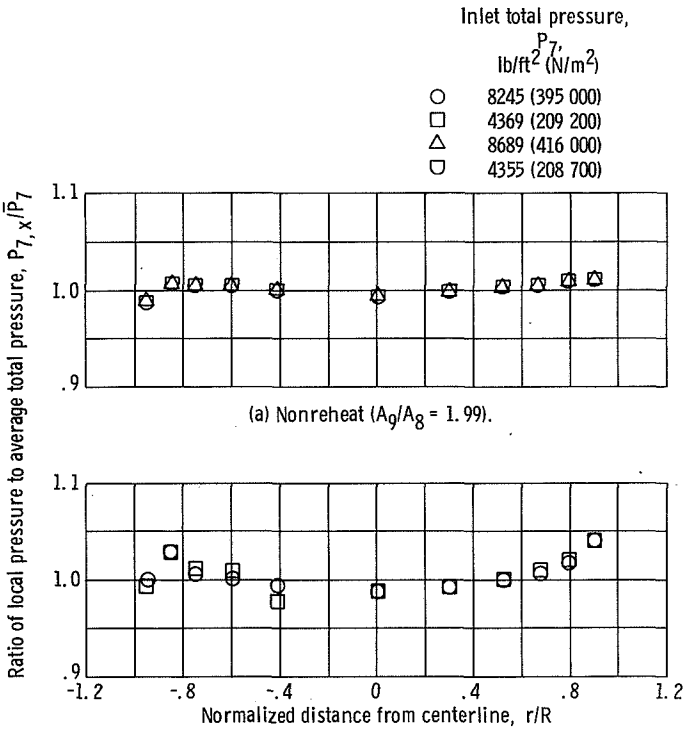

(a) Nonreheat (A_9/A_8 = 1.99).

(b) Maximum reheat (A_9/A_8 = 1.42).

Figure 6. - Primary total-pressure profile at station 7.

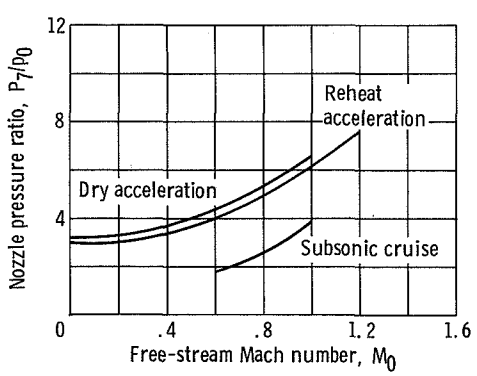

Figure 7. - Schedule of turbojet nozzle pressure ratio with free-stream Mach number.

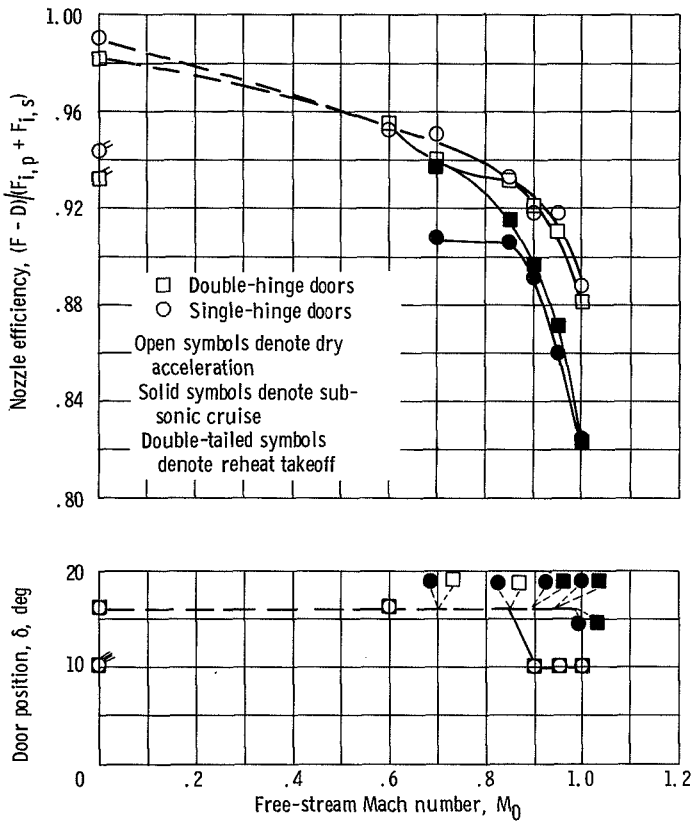

Figure 8. - Comparison of best measured nozzle efficiencies of single- and double-hinge door configurations. Corrected secondary-weight-flow-rate ratio, $\omega\sqrt{\tau} = 0.04$. (Double-hinge door position is denoted by downstream door position δ_2.)

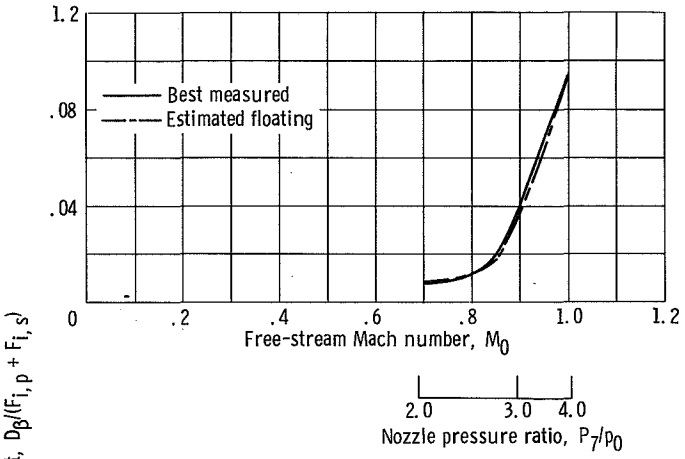

(a) Subsonic cruise (A_9/A_8 = 1.99).

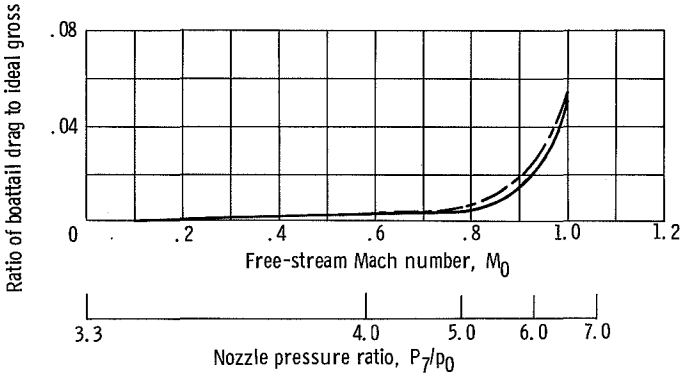

(b) Dry acceleration (A_9/A_8 = 1.99).

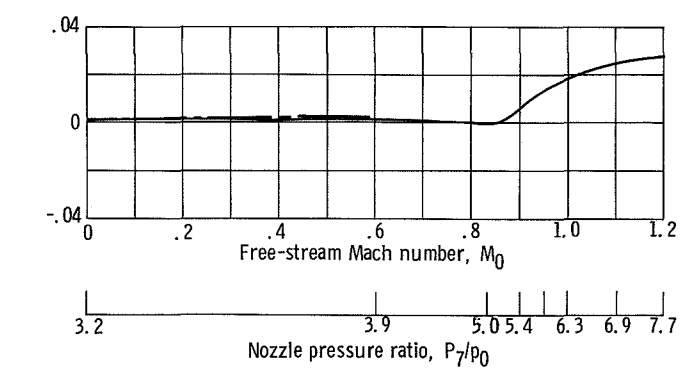

(c) Maximum reheat acceleration (A_9/A_8 = 1.42).

Figure 9. - Comparison of boattail drag to ideal gross thrust, for single- and double-hinge doors.

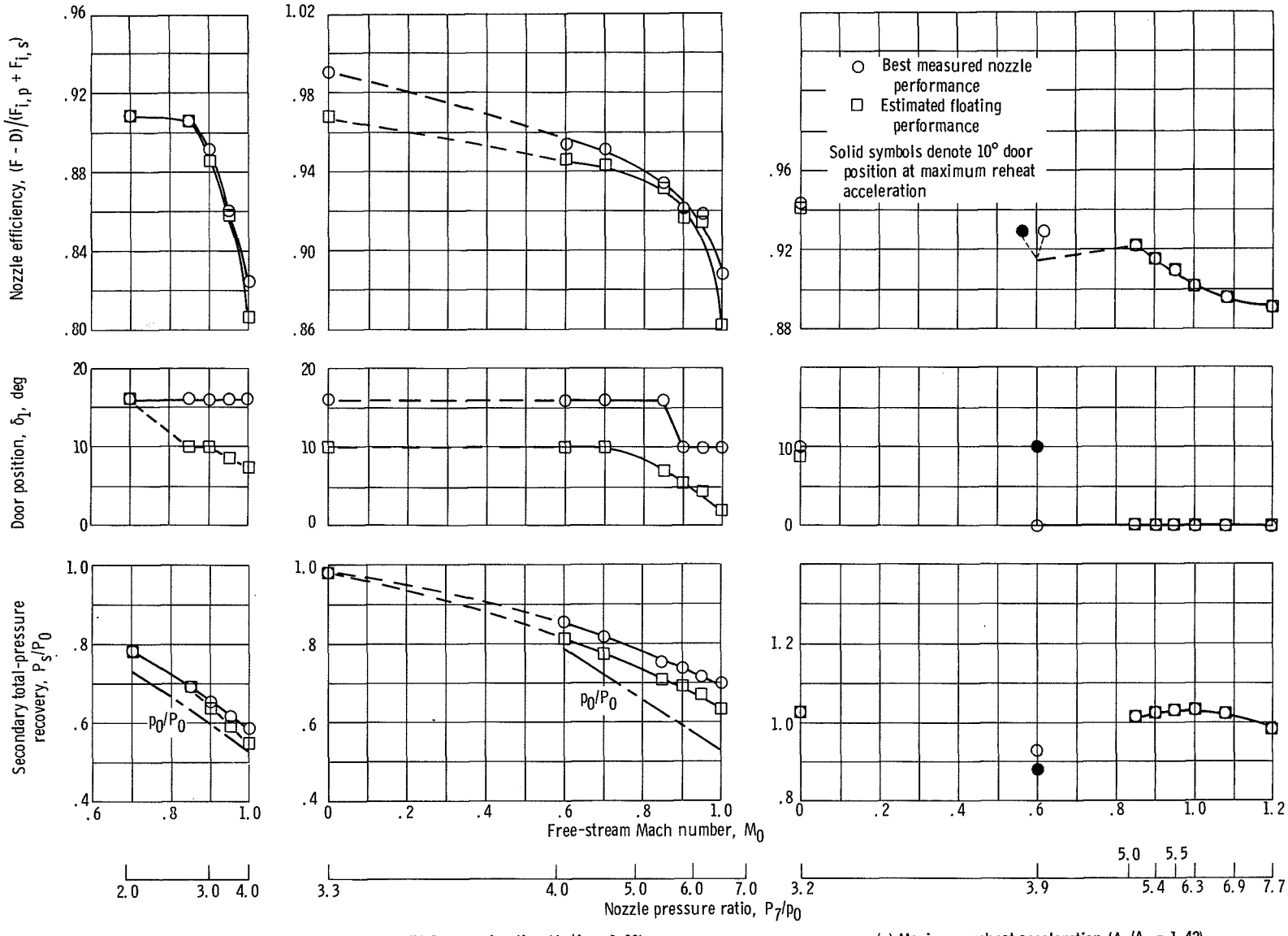

(a) Subsonic cruise (A_9/A_8 = 1.99).

(b) Dry acceleration (A_9/A_8 = 1.99).

(c) Maximum reheat acceleration (A_9/A_8 = 1.42).

Figure 10. - Performance and total-pressure-recovery requirements of single-hinge door configurations. Corrected secondary-weight-flow-rate ratio, $\omega\sqrt{\tau}$ = 0.04.

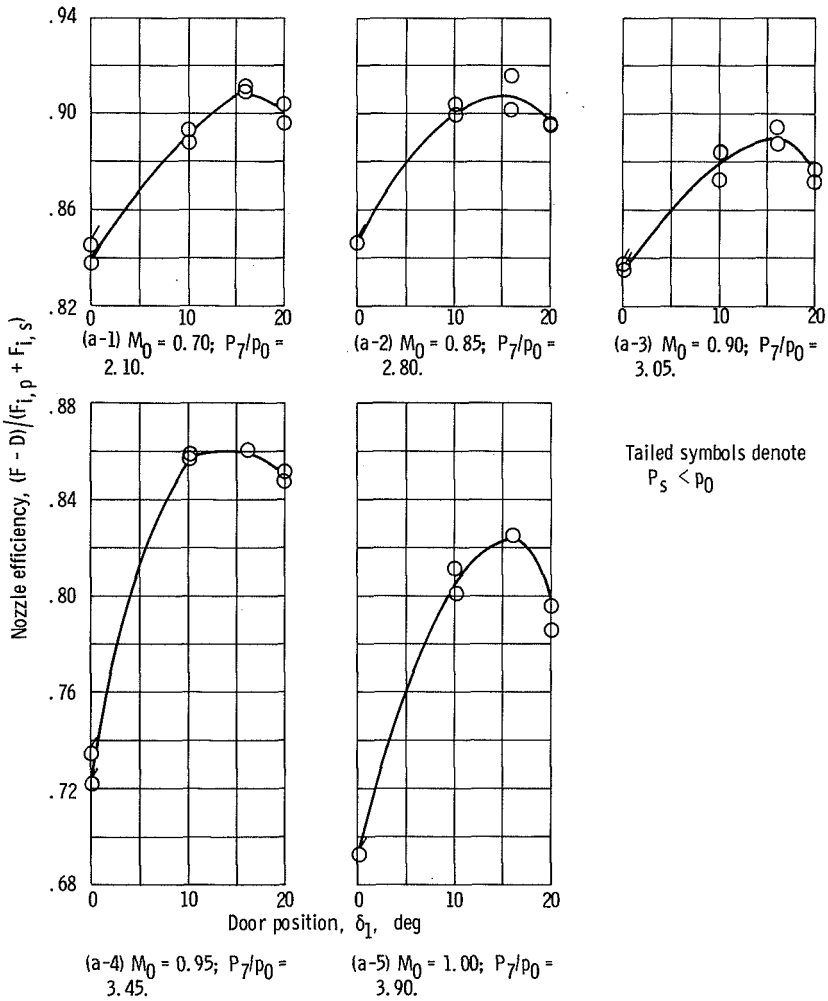

(a) Subsonic cruise ($A_9/A_8 = 1.99$).

Figure 11. - Effect of single-hinge door position on nozzle efficiency.

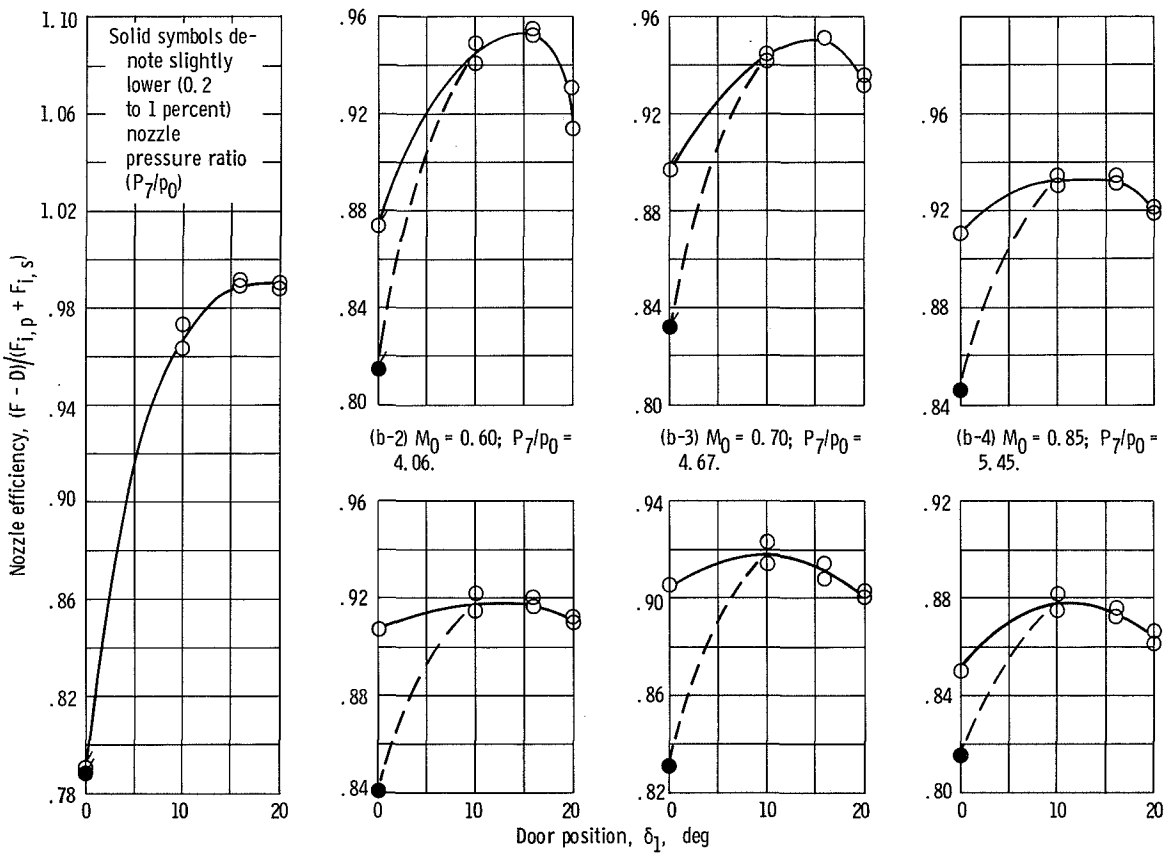

(b-1) $M_0 = 0$; $P_7/p_0 = 3.30$.

(b-2) $M_0 = 0.60$; $P_7/p_0 = 4.06$.

(b-3) $M_0 = 0.70$; $P_7/p_0 = 4.67$.

(b-4) $M_0 = 0.85$; $P_7/p_0 = 5.45$.

(b-5) $M_0 = 0.90$; $P_7/p_0 = 5.70$.

(b-6) $M_0 = 0.95$; $P_7/p_0 = 6.28$.

(b-7) $M_0 = 1.00$; $P_7/p_0 = 6.65$.

(b) Dry acceleration ($A_9/A_8 = 1.99$).

Figure 11. - Continued.

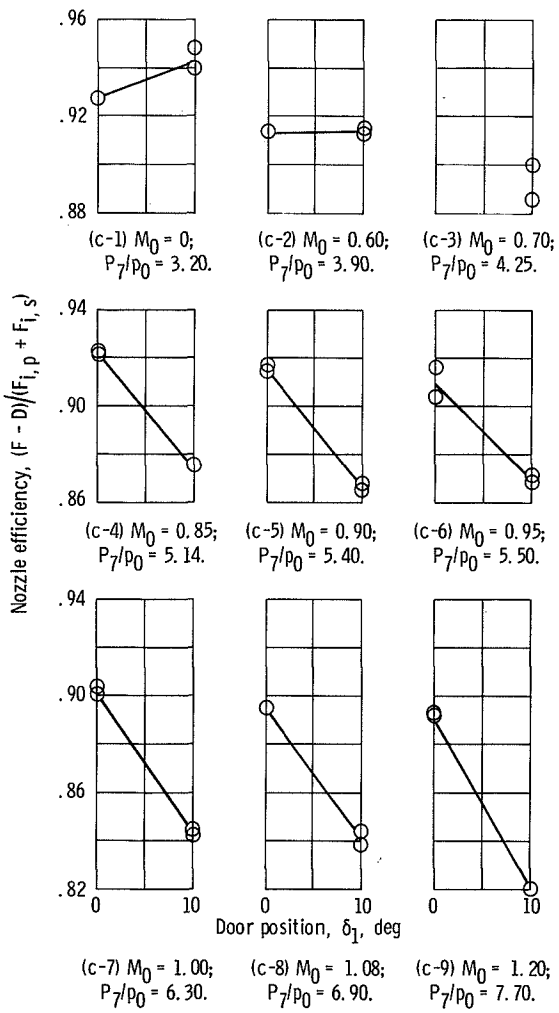

(c) Maximum reheat acceleration (A_9/A_8 = 1.42).

Figure 11. - Concluded.

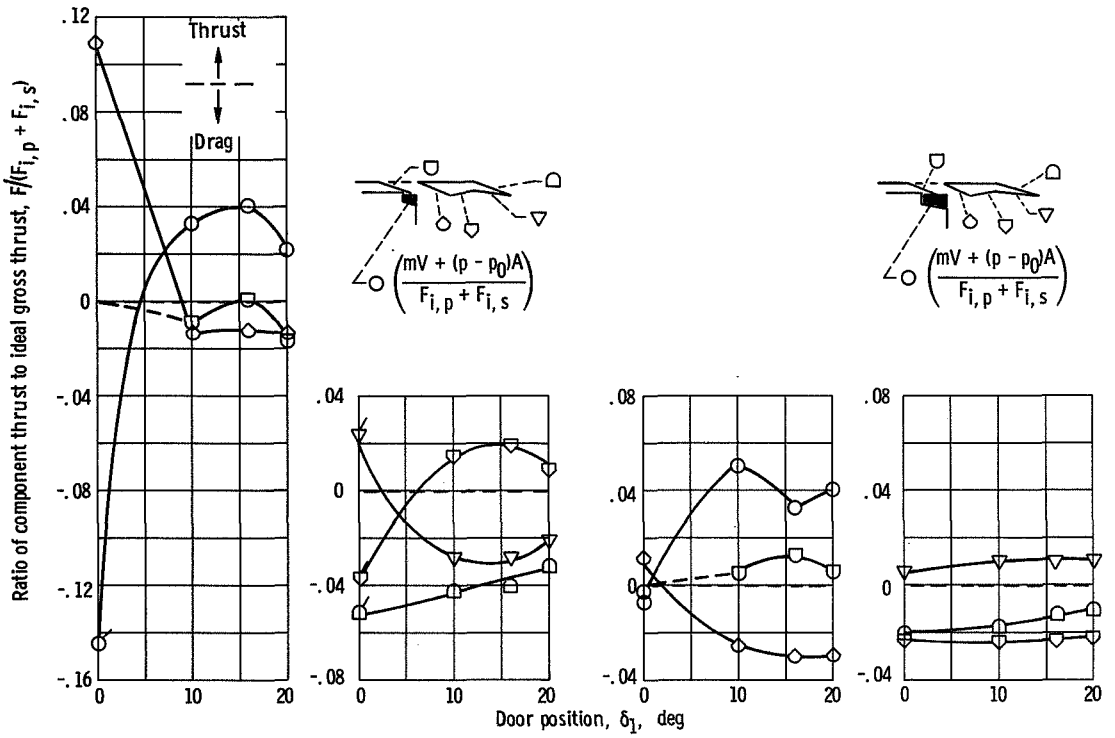

(a) Subsonic cruise (A_9/A_8 = 1.99); nozzle pressure ratio, P_7/p_0 = 3.05.

(b) Dry acceleration (A_9/A_8 = 1.99); nozzle pressure ratio, P_7/p_0 = 5.70.

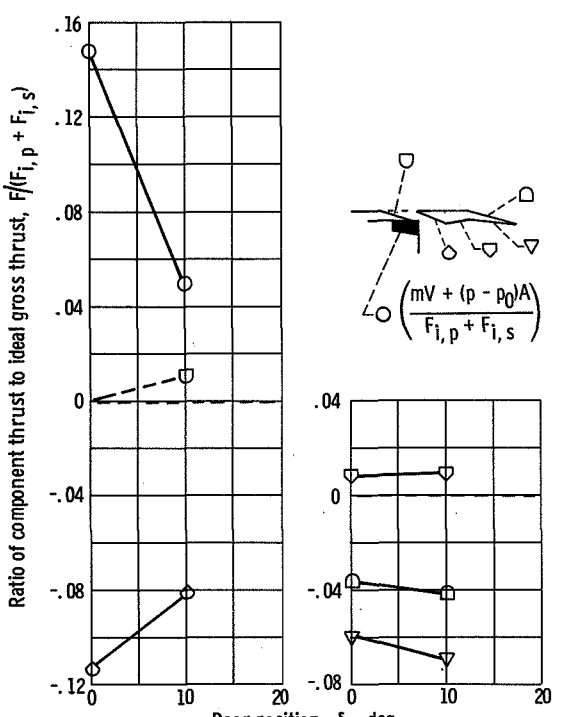

(c) Maximum reheat acceleration (A_9/A_8 = 1.42); nozzle pressure ratio, P_7/p_0 = 5.40.

Figure 12. - Effect of single-hinge door position on component thrust to ideal gross-thrust ratio. Corrected secondary-weight-flow-rate ratio, $\omega\sqrt{\theta}$ = 0.04; free-stream Mach number, M_0 = 0.90.

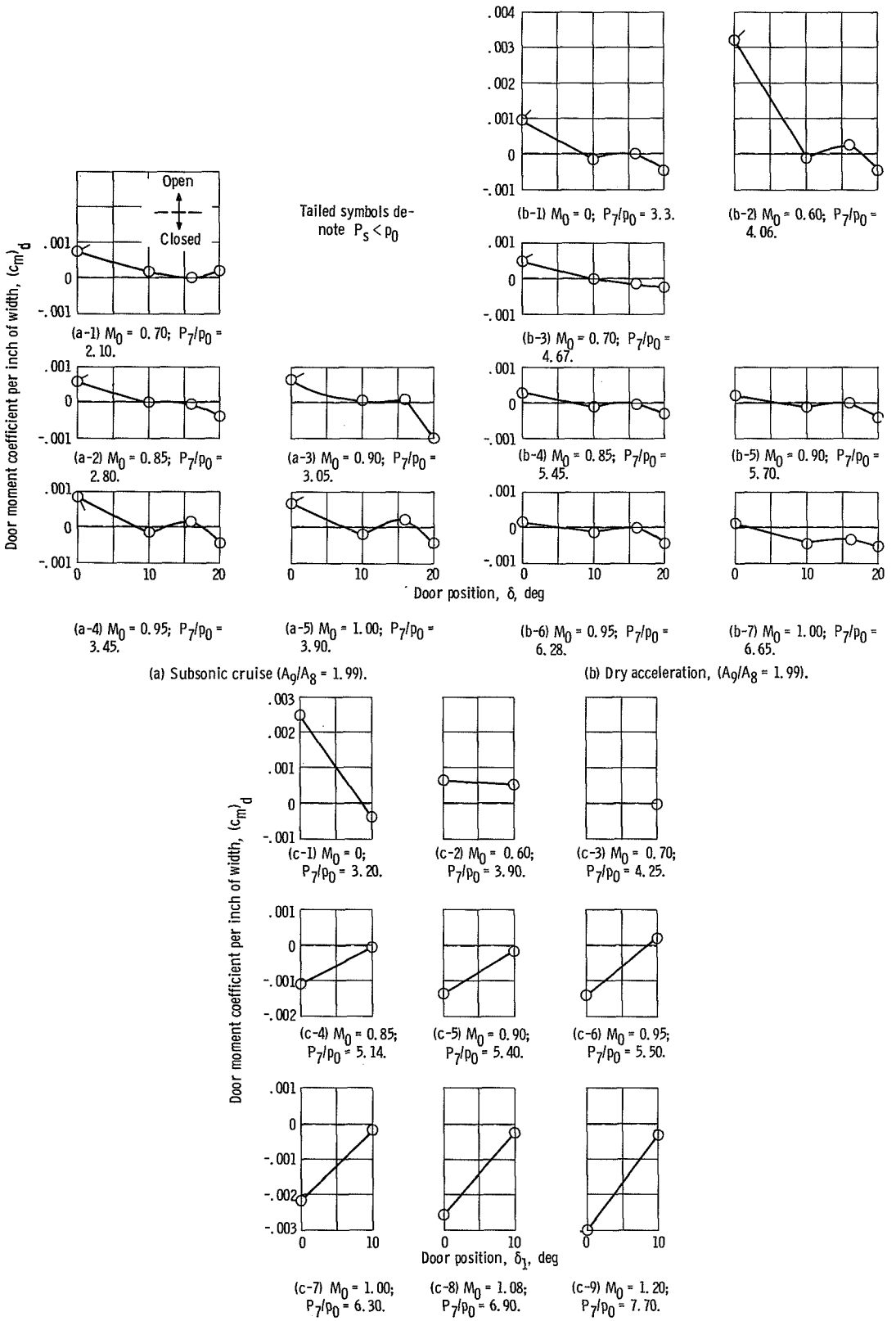

Figure 13. - Effect of single-hinge door position on door moment coefficient. Corrected secondary-weight-flow-rate ratio, $\omega\sqrt{\tau} = 0.04$.

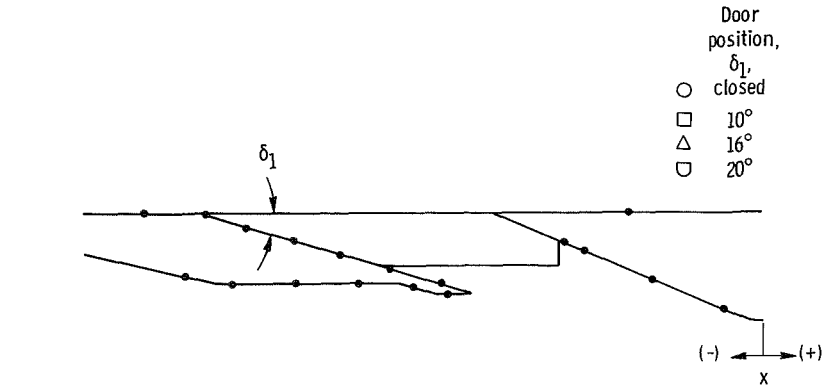

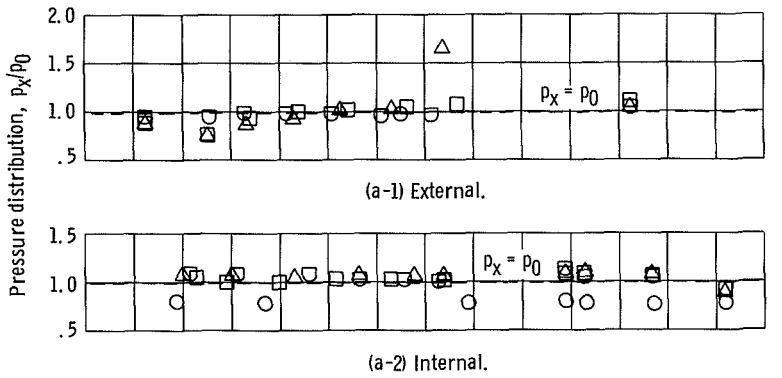

(a-1) External.

(a-2) Internal.

(a) Subsonic cruise (A_9/A_8 = 1.99); nozzle pressure ratio, P_7/p_0 = 3.05 free-stream Mach number, M_0 = 0.90.

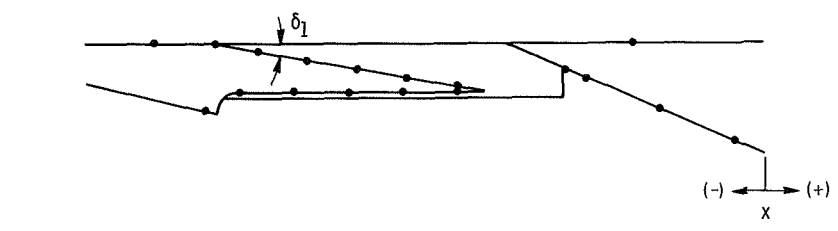

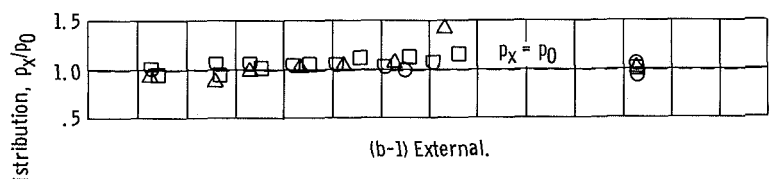

(b-1) External.

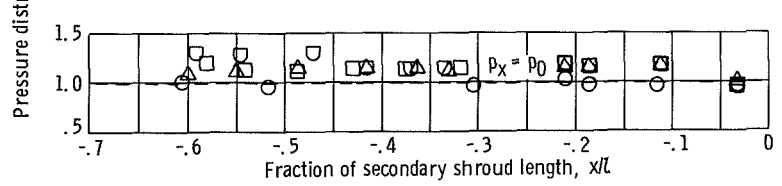

(b-2) Internal.

(b) Dry acceleration (A_9/A_8 = 1.99); nozzle pressure ratio, P_7/p_0 = 5.7; Mach number, M_0 = 0.90.

Figure 14. - Effect of single-hinge door position on auxiliary inlet pressure distribution. Corrected secondary-weight-flow-rate ratio, $\omega\sqrt{\tau}$ = 0.04.

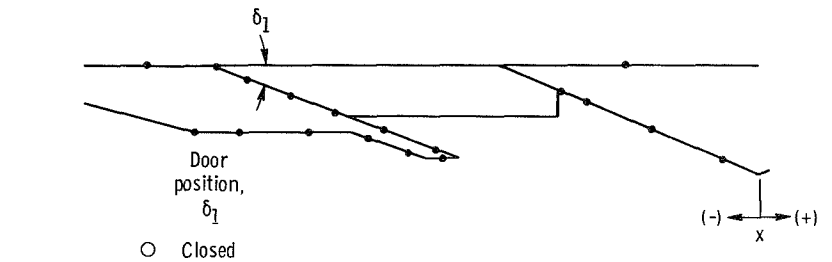

○ Closed
□ 10°

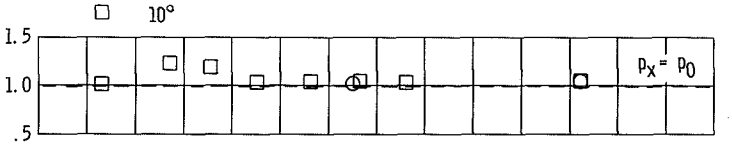

(c-1) External.

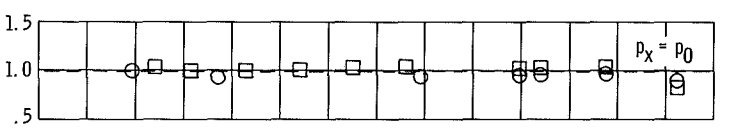

(c-2) Internal.

(c) Maximum reheat acceleration (A_9/A_8 = 1.42); nozzle pressure ratio, P_7/p_0 = 3.2; free-stream Mach number, M_0 = 0.

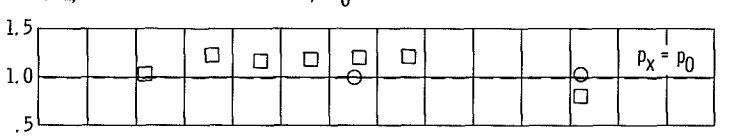

(d-1) External.

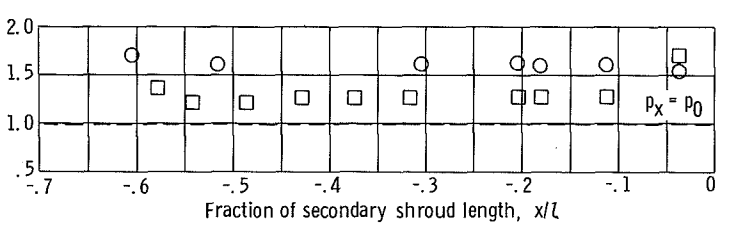

(d-2) Internal.

(d) Maximum reheat acceleration (A_9/A_8 = 1.42); nozzle pressure ratio, P_7/p_0 = 5.5; free-stream Mach number, M_0 = 0.95.

Pressure distribution, p_x/p_0

Figure 14. - Concluded.

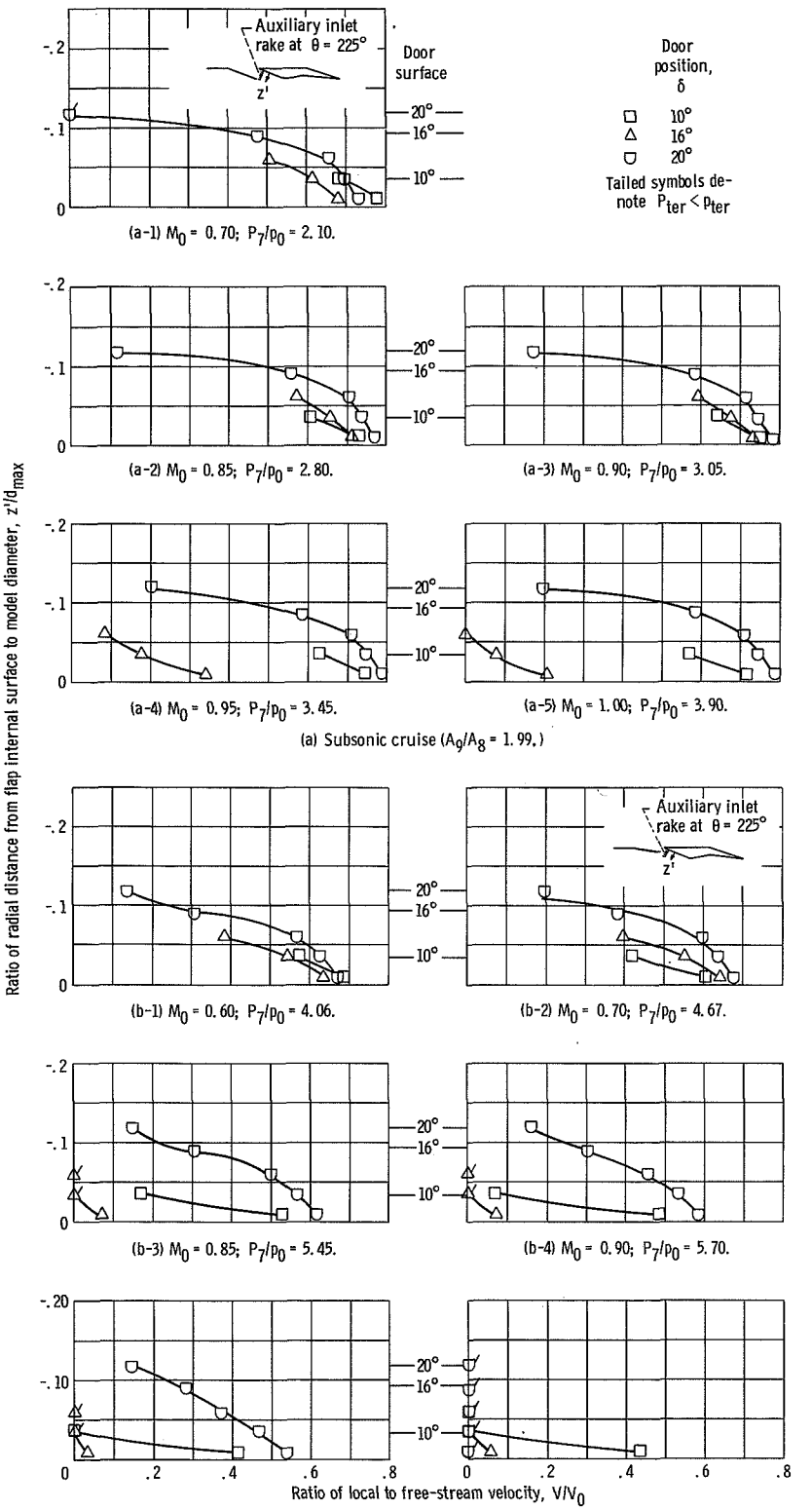

Figure 15. - Effect of single-hinge door position on auxiliary inlet flow velocity. Corrected secondary-weight-flow-rate ratio, $\omega\sqrt{\tau}$ = 0.04.

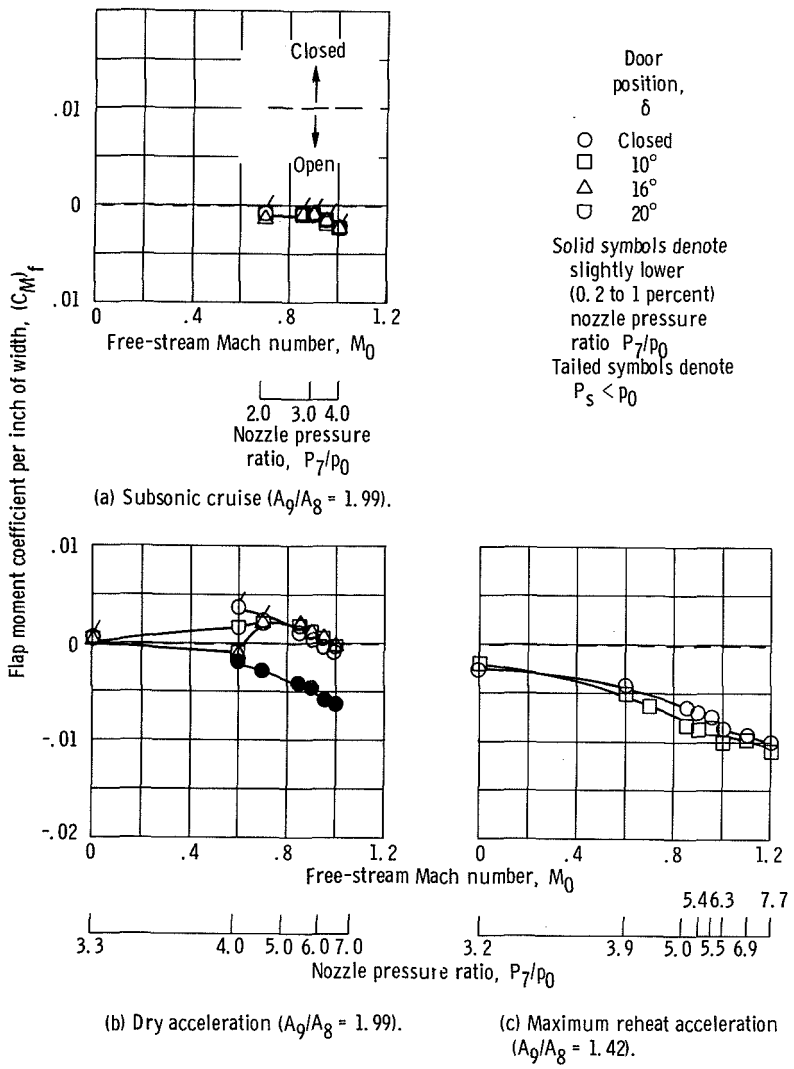

(a) Subsonic cruise (A_9/A_8 = 1.99).

(b) Dry acceleration (A_9/A_8 = 1.99).

(c) Maximum reheat acceleration (A_9/A_8 = 1.42).

Figure 16. - Effect of single-hinge door position on trailing-edge flap moment coefficient. Corrected secondary-weight-flow-rate ratio, $\omega\sqrt{\tau}$ = 0.04.

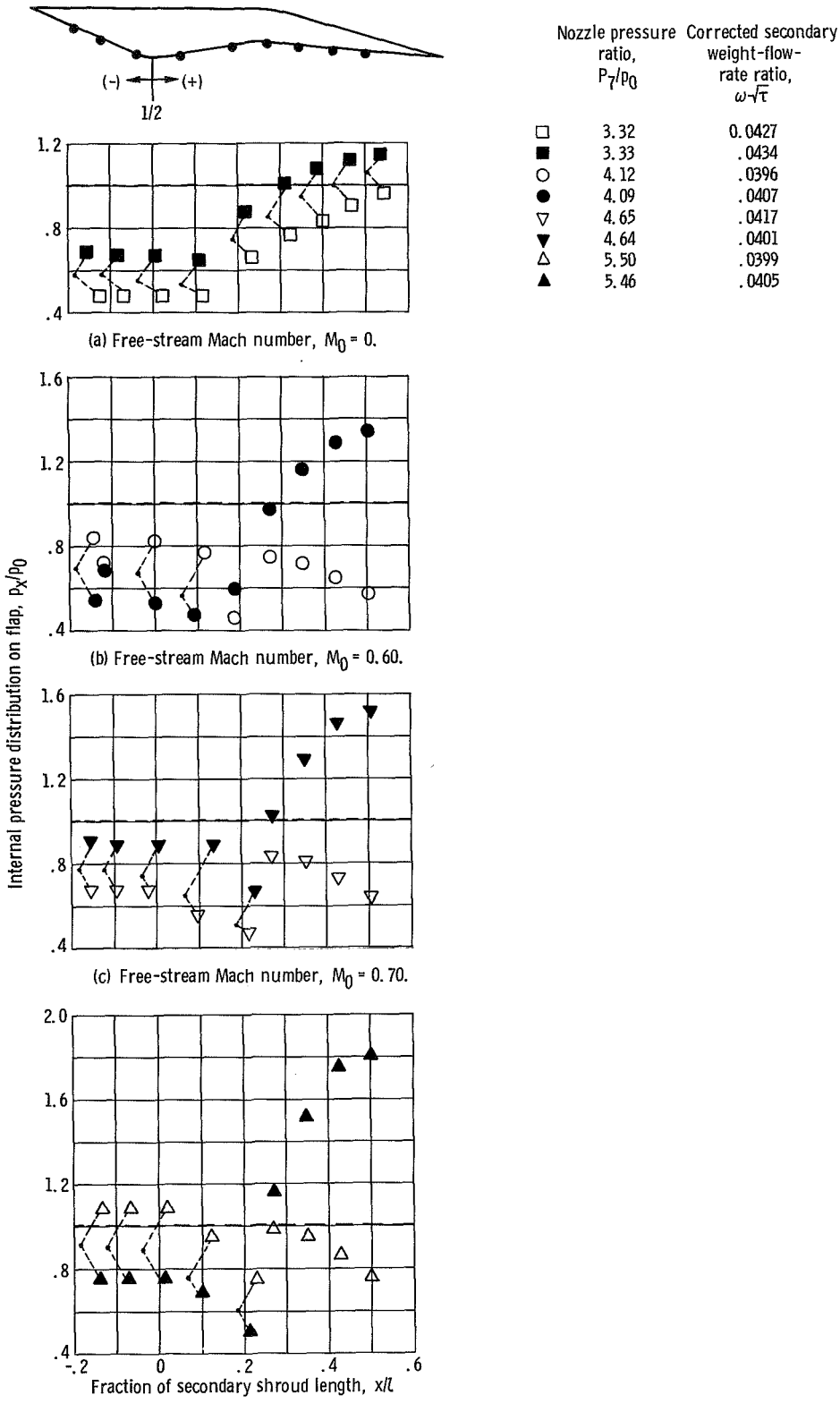

(a) Free-stream Mach number, $M_0 = 0$.

(b) Free-stream Mach number, $M_0 = 0.60$.

(c) Free-stream Mach number, $M_0 = 0.70$.

(d) Free-stream Mach number, $M_0 = 0.85$.

Figure 17. - Effect of nozzle pressure ratio on flap internal pressure distribution with doors closed. Dry acceleration ($A_9/A_8 = 1.99$).

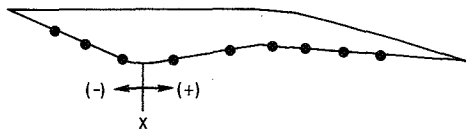

Nozzle pressure ratio, P_7/p_0	Corrected secondary-weight-flow-rate ratio, $\omega\sqrt{\tau}$
5.81	0.0399
5.75	.0411
6.35	.0396
6.31	.0396
6.58	.0404
6.52	.0403

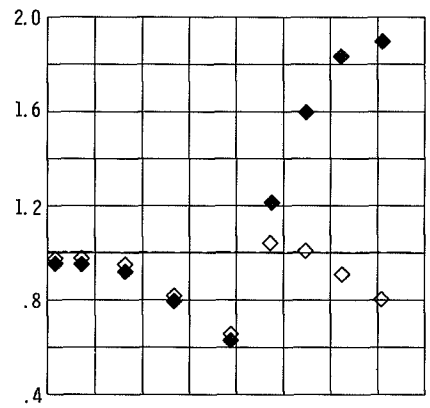

(e) Free-stream Mach number, $M_0 = 0.90$.

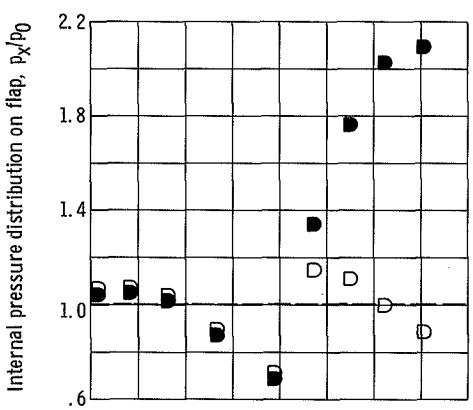

(f) Free-stream Mach number, $M_0 = 0.95$.

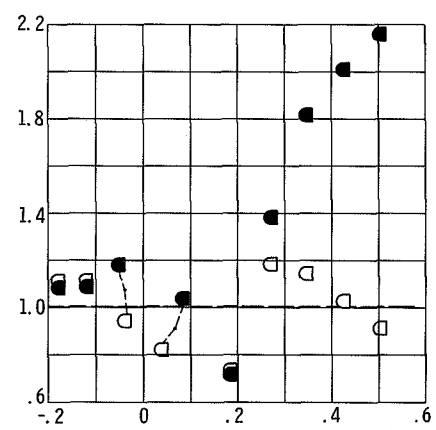

(g) Free-stream Mach number, $M_0 = 1.00$.

Figure 17. - Concluded.

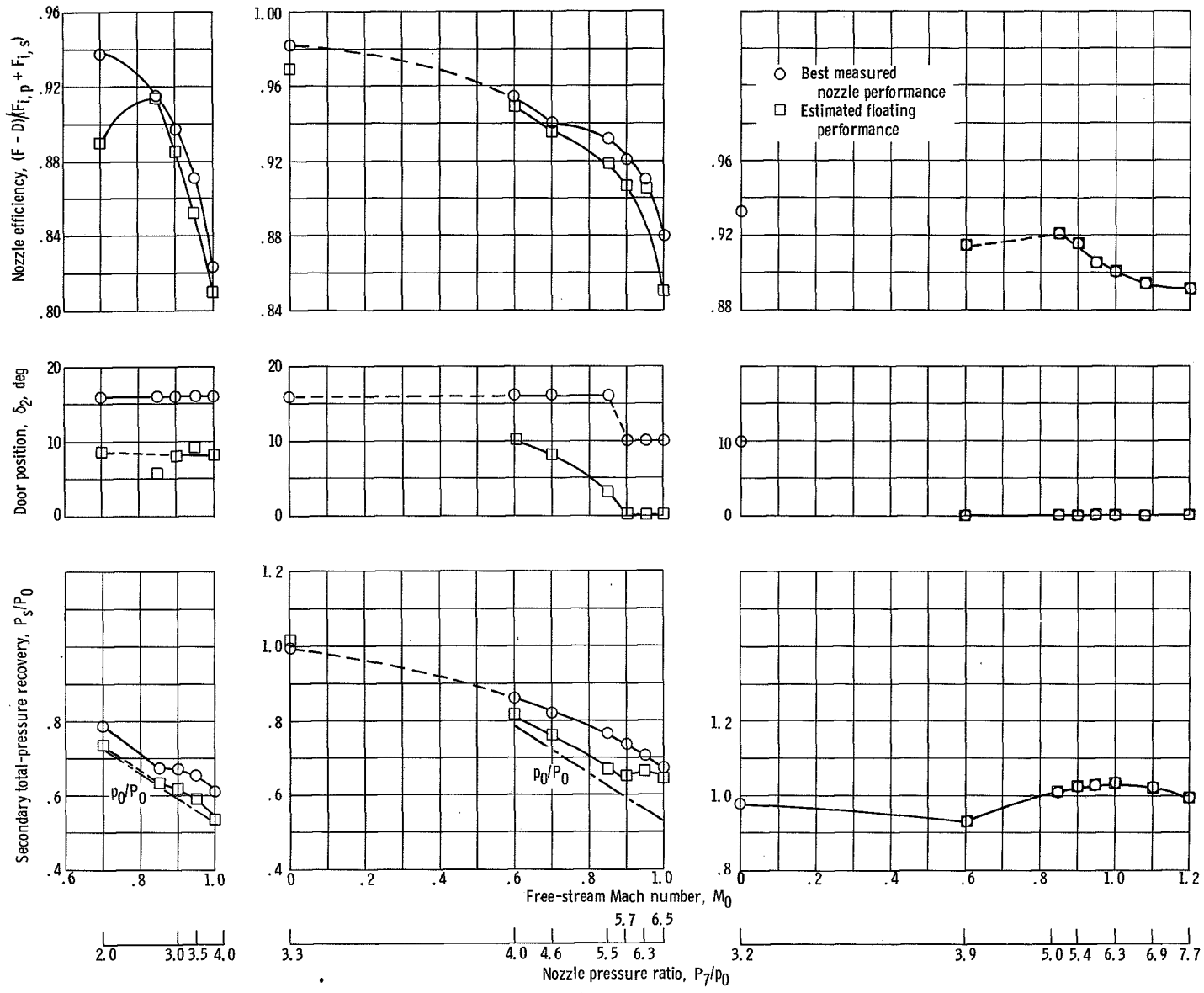

(a) Subsonic cruise (A_9/A_8 = 1.99).

(b) Dry acceleration (A_9/A_8 = 1.99.)

(c) Maximum reheat acceleration (A_9/A_8 = 1.42).

Figure 18. - Performance and total-pressure-recovery requirements of double-hinge door configurations. Corrected secondary-weight-flow-rate ratio, $\omega\sqrt{\tau}$ = 0.04.

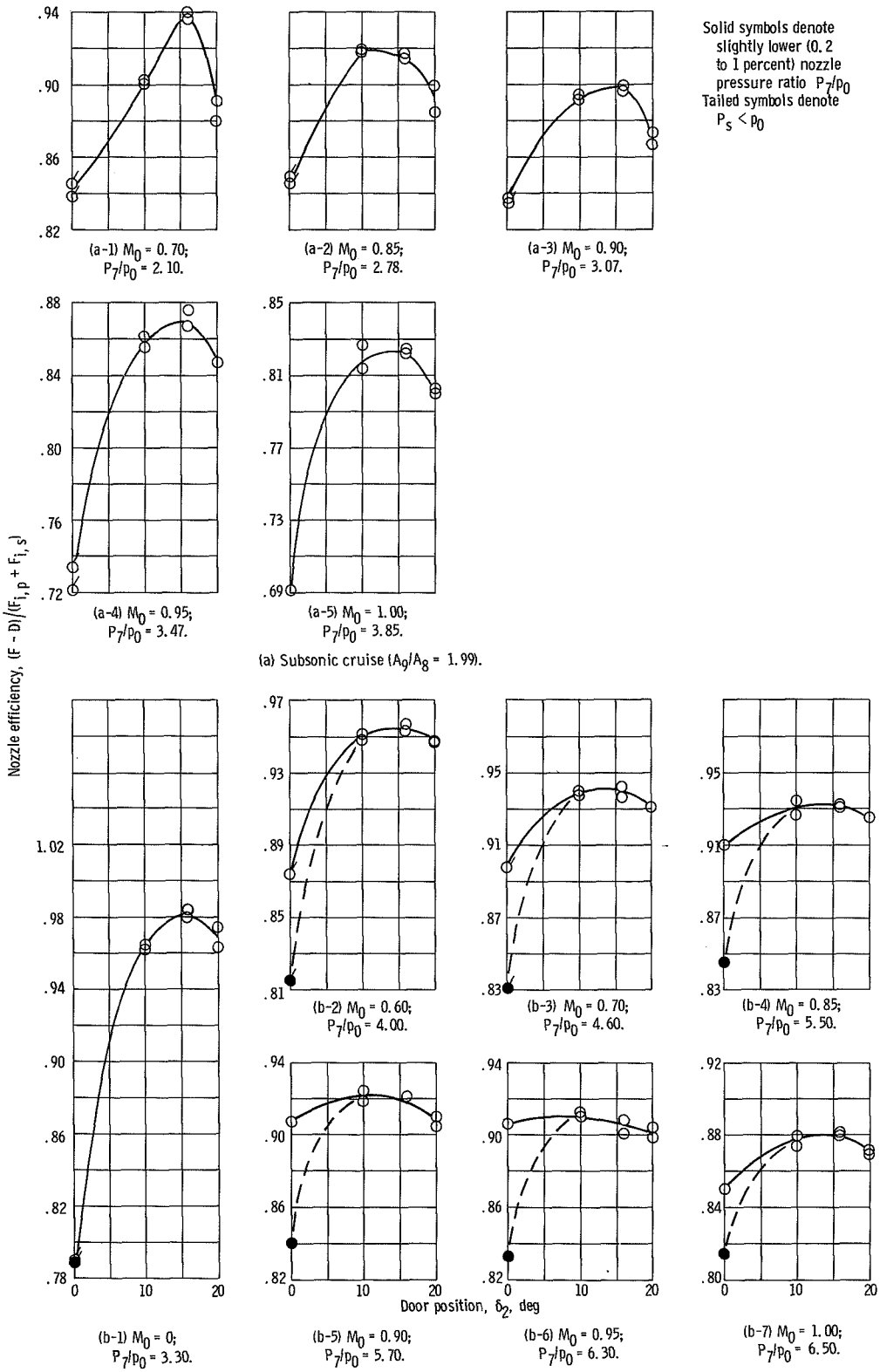

Figure 19. - Effect of double-hinge door position on nozzle efficiency. Corrected secondary-weight-flow-rate ratio, $\omega\sqrt{\tau}$ = 0.04.

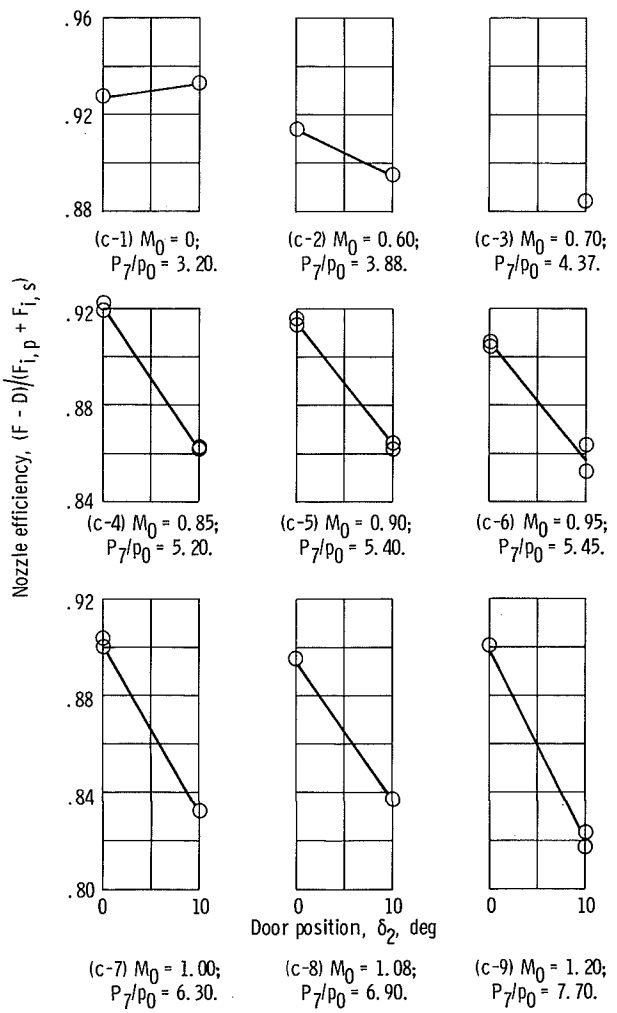

(c) Maximum reheat acceleration (A_9/A_8 = 1.42).

Figure 19. - Concluded.

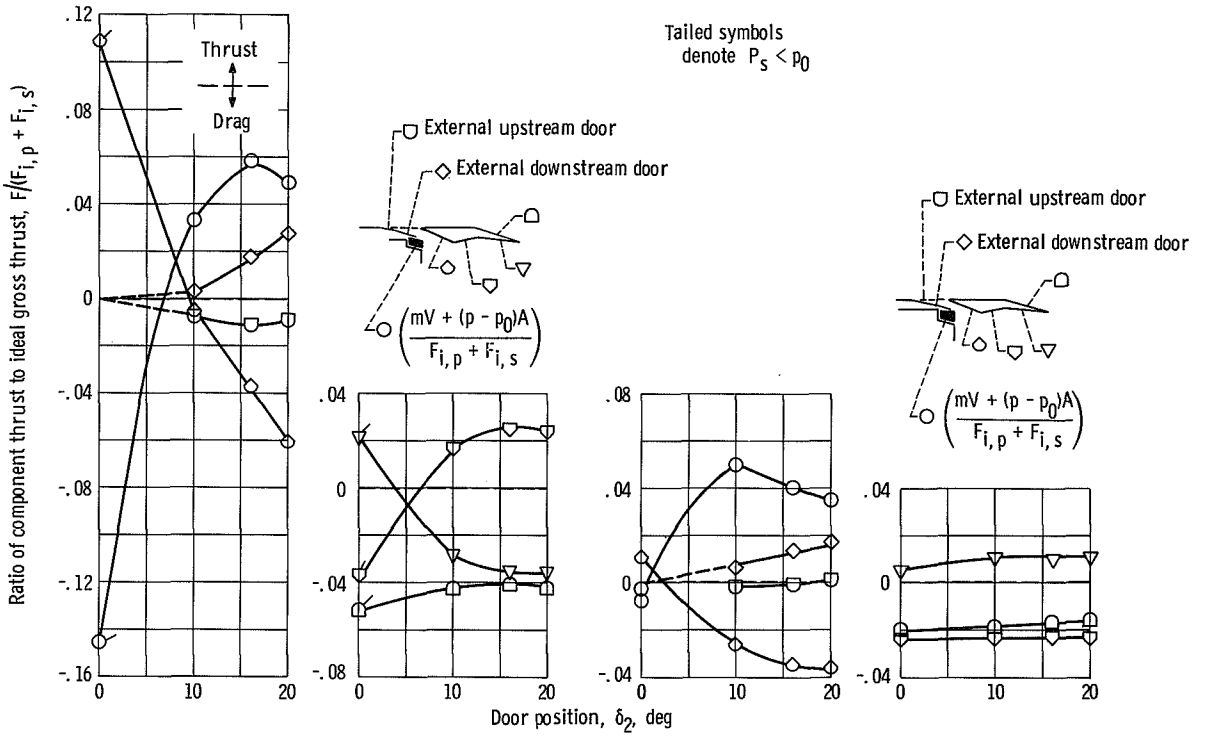

(a) Subsonic cruise (A_9/A_8 = 1.99); nozzle pressure ratio, P_7/p_0 = 3.07.

(b) Dry acceleration (A_9/A_8 = 1.99); nozzle pressure ratio, P_7/p_0 = 5.70.

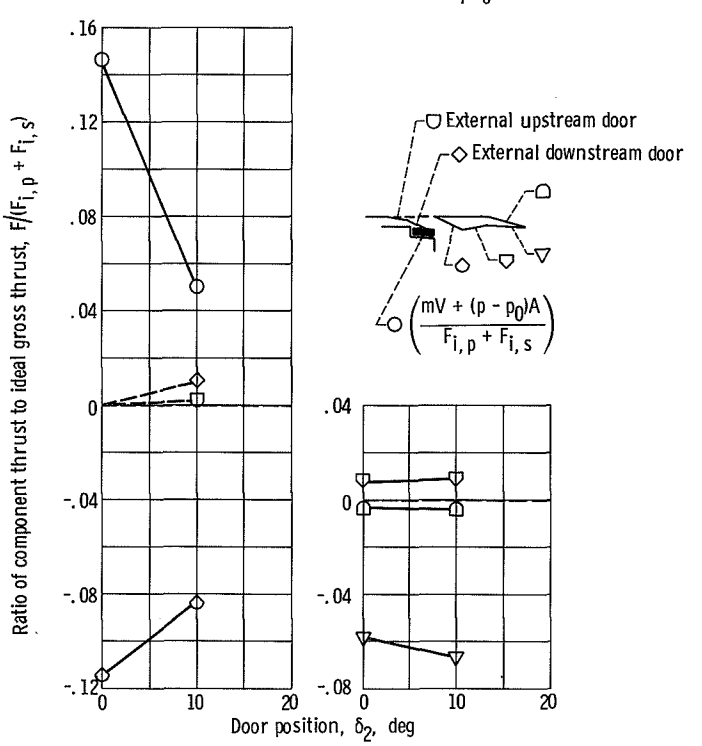

(c) Maximum reheat acceleration (A_9/A_8 = 1.42); nozzle pressure ratio, P_7/p_0 = 5.40.

Figure 20. - Effect of double-hinge door position on component thrust to ideal gross-thrust ratio. Corrected secondary-weight-flow-rate ratio, $\omega\sqrt{\tau}$ = 0.04; free-stream Mach number, M_0 = 0.90.

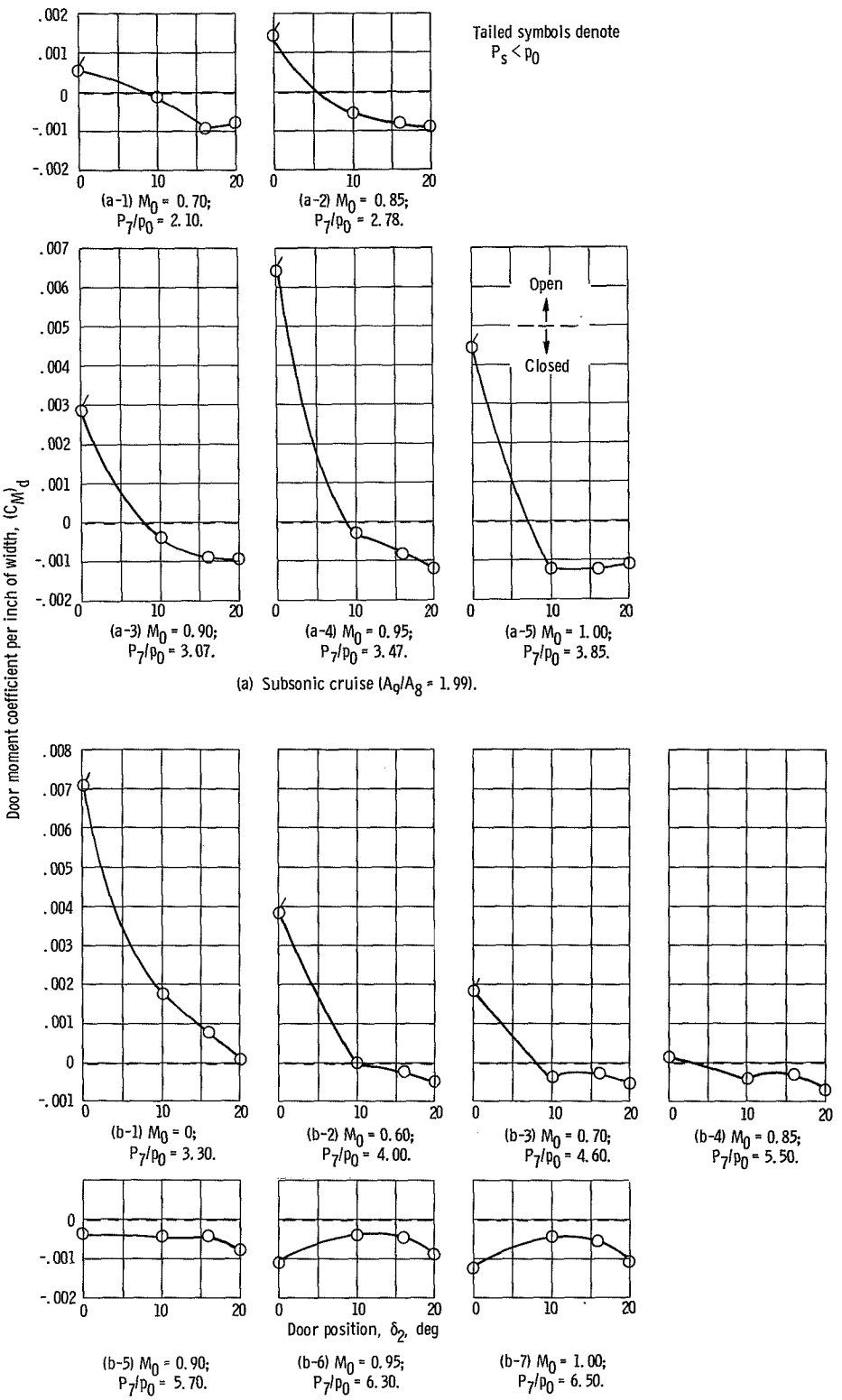

Figure 21. - Effect of double-hinge door position on door moment coefficient. Corrected secondary-weight-flow-rate ratio, $\omega\sqrt{\tau}$ = 0.04.

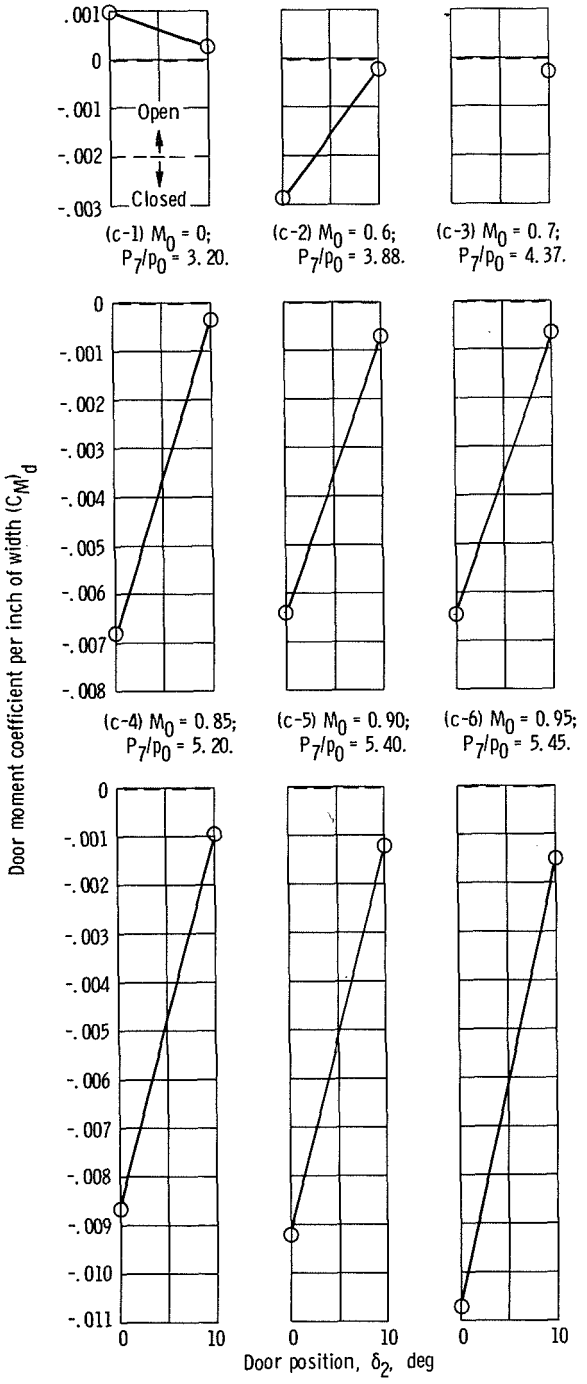

(c) Maximum reheat acceleration (A_9/A_8 = 1.42).

Figure 21. - Concluded.

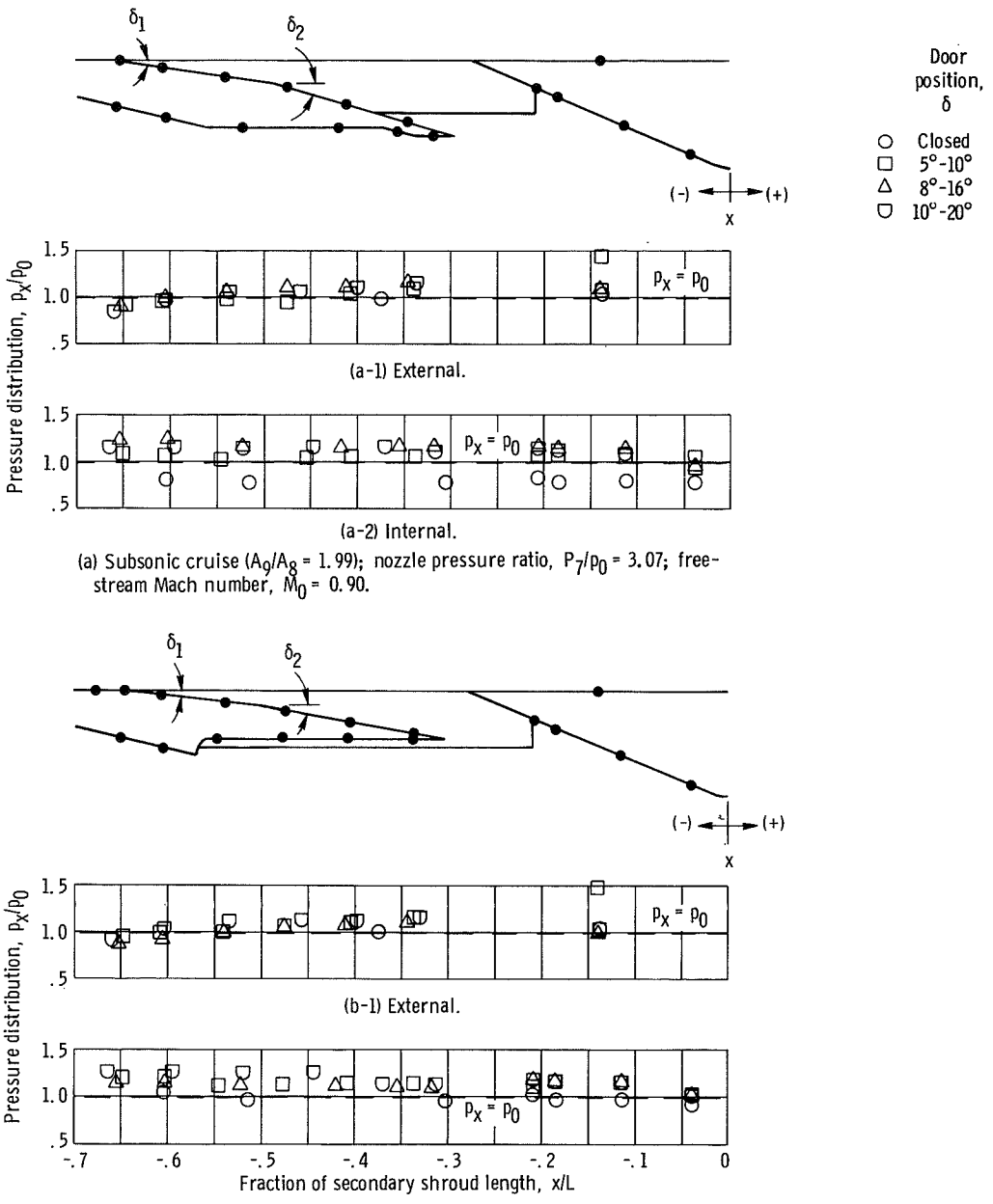

(a) Subsonic cruise (A_9/A_8 = 1.99); nozzle pressure ratio, P_7/p_0 = 3.07; free-stream Mach number, M_0 = 0.90.

(b) Dry acceleration (A_9/A_8 = 1.99); nozzle pressure ratio, P_7/p_0 = 5.7; free-stream Mach number, M_0 = 0.90.

Figure 22. - Effect of double-hinge door position on auxiliary inlet pressure distribution. Corrected secondary-weight-flow-rate ratio, $\omega\sqrt{\tau}$ = 0.04.

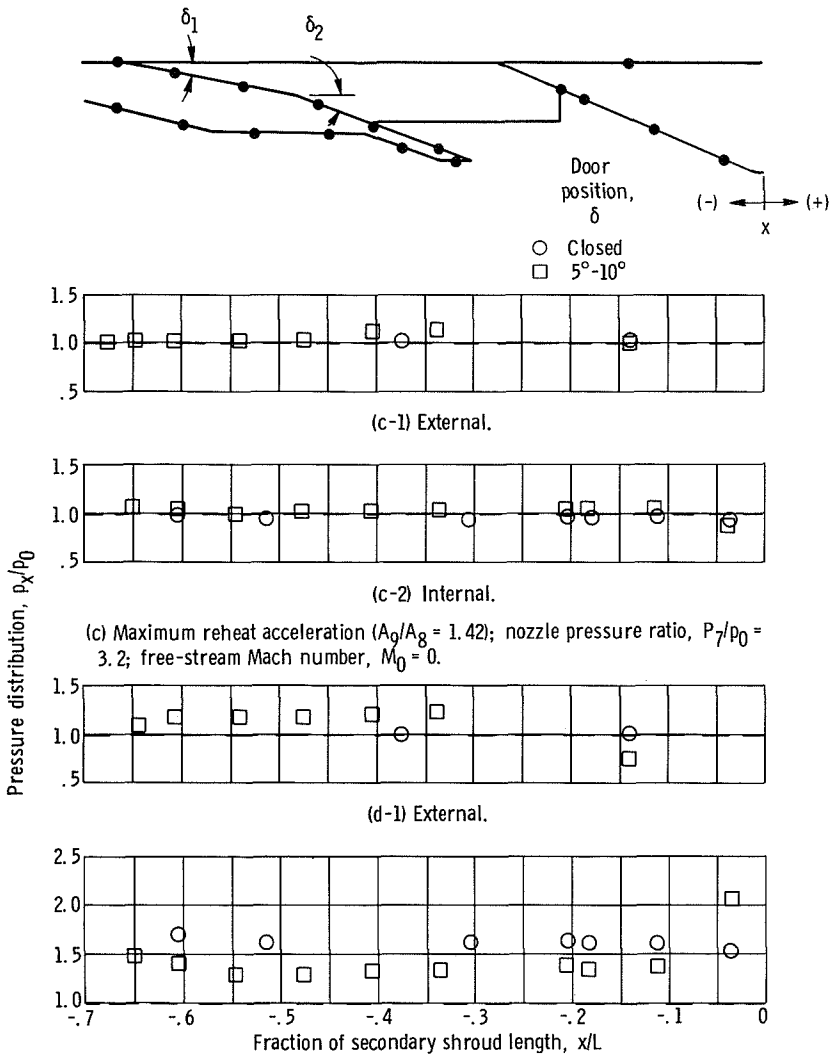

(c) Maximum reheat acceleration (A_9/A_8 = 1.42); nozzle pressure ratio, P_7/p_0 = 3.2; free-stream Mach number, M_0 = 0.

(d) Maximum reheat acceleration (A_9/A_8 = 1.42); nozzle pressure ratio, P_7/p_0 = 5.45; free-stream Mach number, M_0 = 0.95.

Figure 22. - Concluded.

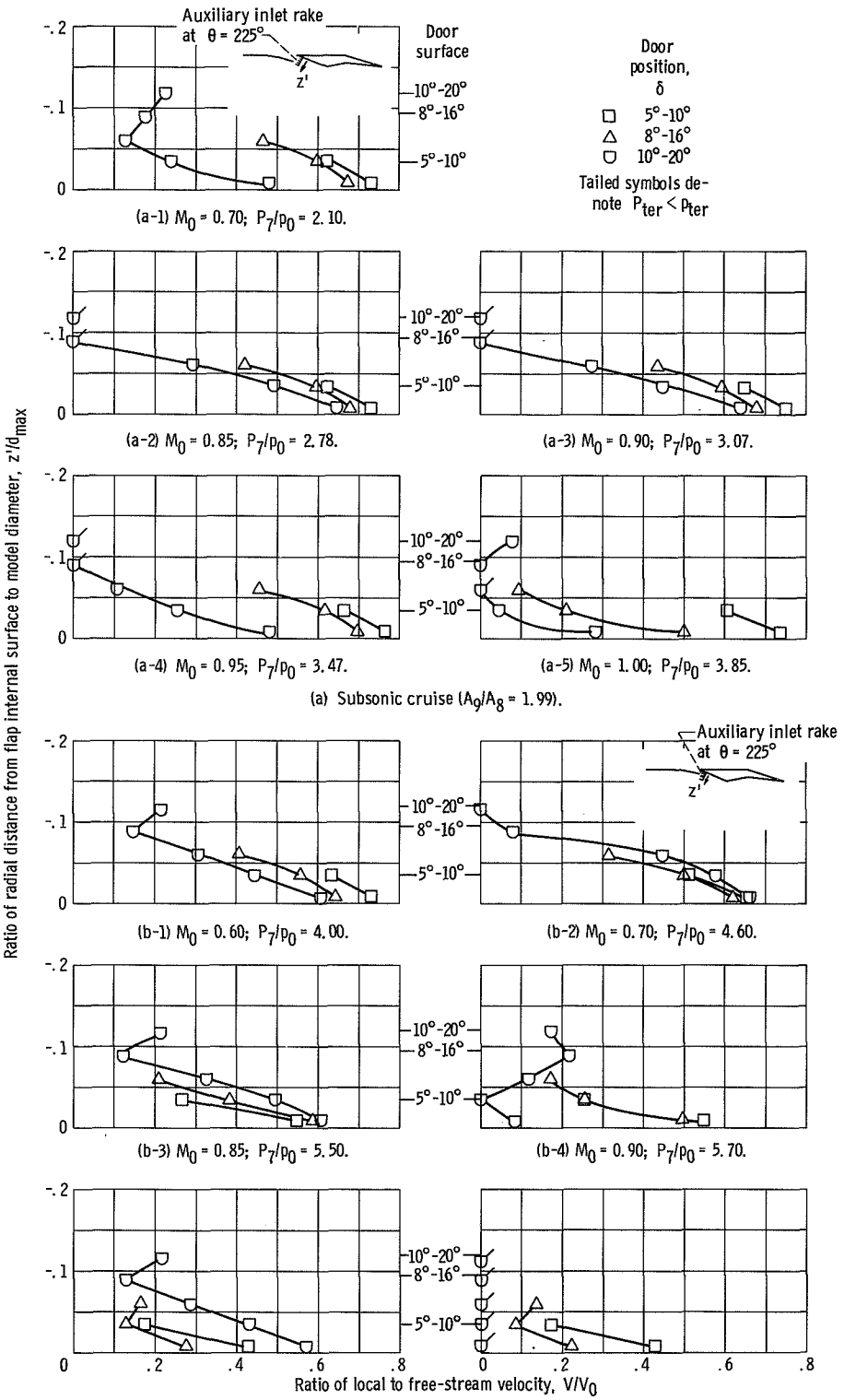

Figure 23. - Effect of double-hinge door position on auxiliary inlet flow velocity. Corrected secondary-weight-flow-rate ratio, $\omega\sqrt{\theta}$ = 0.04.

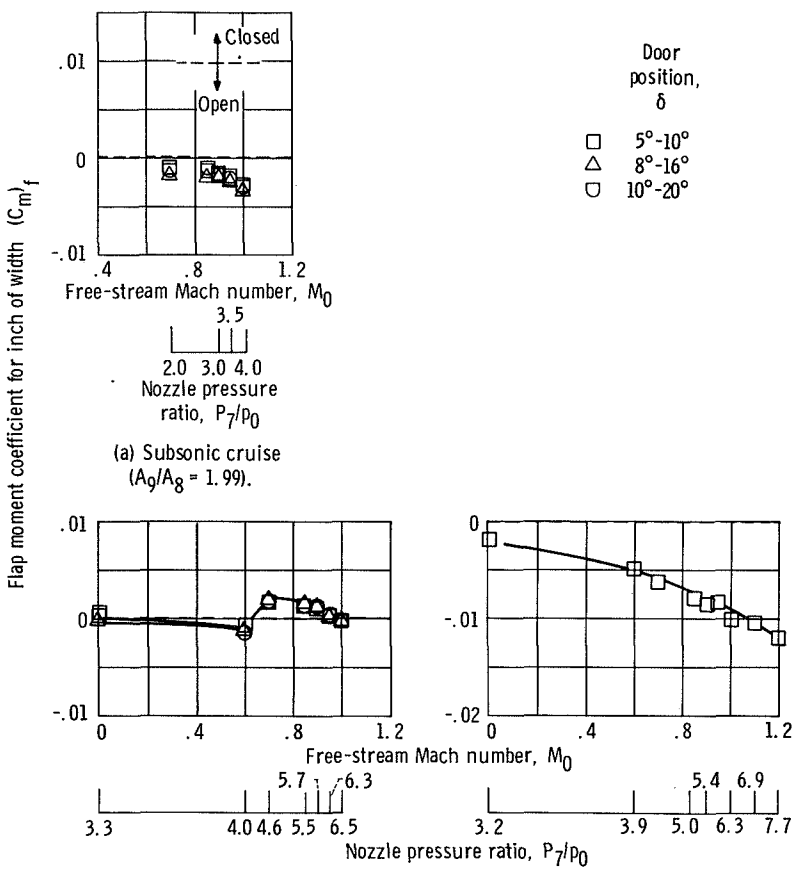

(a) Subsonic cruise (A_9/A_8 = 1.99).

(b) Dry acceleration (A_9/A_8 = 1.99).

(c) Maximum reheat acceleration (A_9/A_8 = 1.42).

Figure 24. - Effect of double-hinge door position on trailing-edge flap moment coefficient. Corrected secondary-weight-flow-rate ratio, $\omega\sqrt{\tau}$ = 0.04.

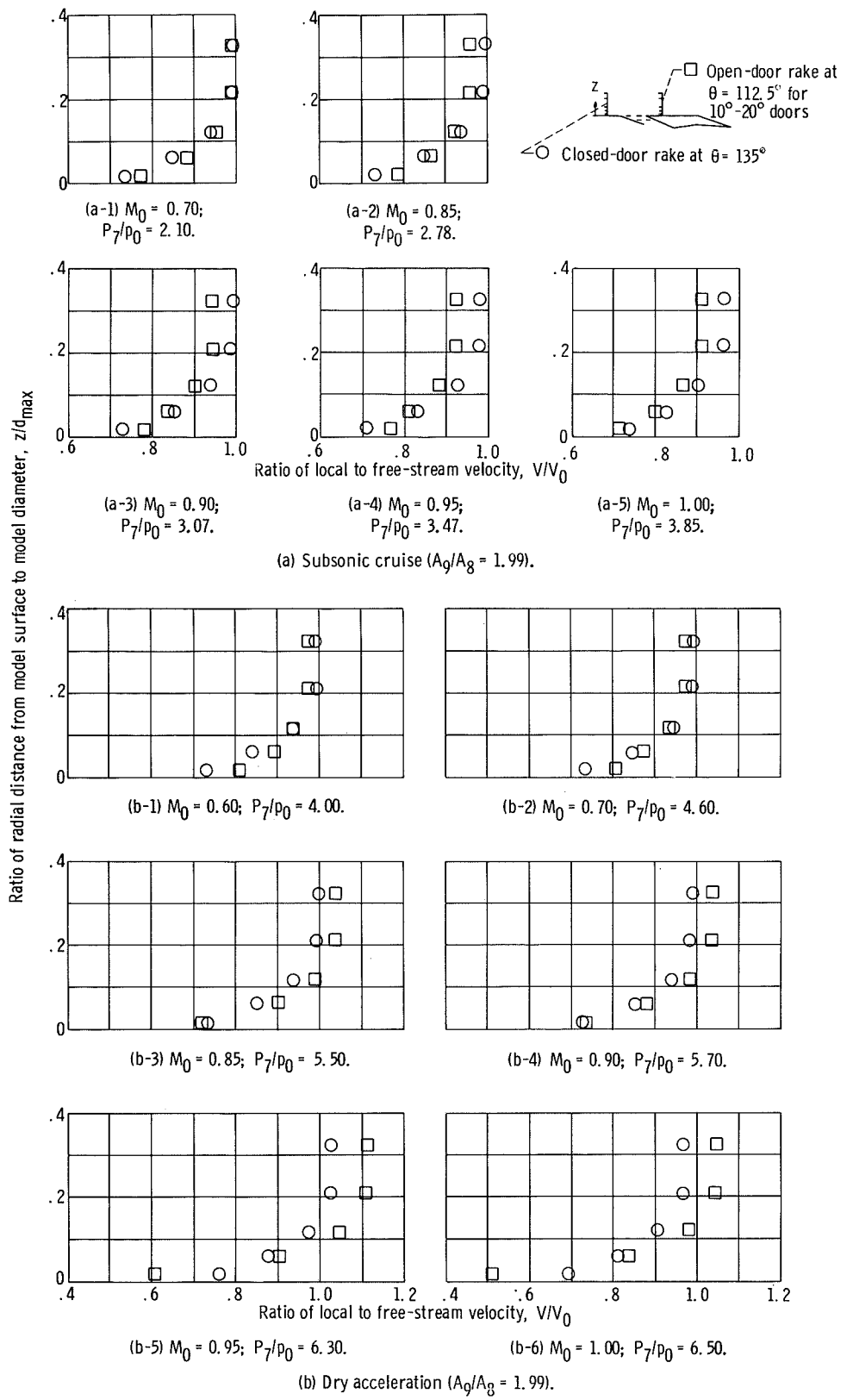

Figure 25. - Comparison of afterbody boundary-layer characteristics for closed and full-open door positions. Corrected secondary-weight-flow-rate ratio, $\omega\sqrt{\tau}$ = 0.04.

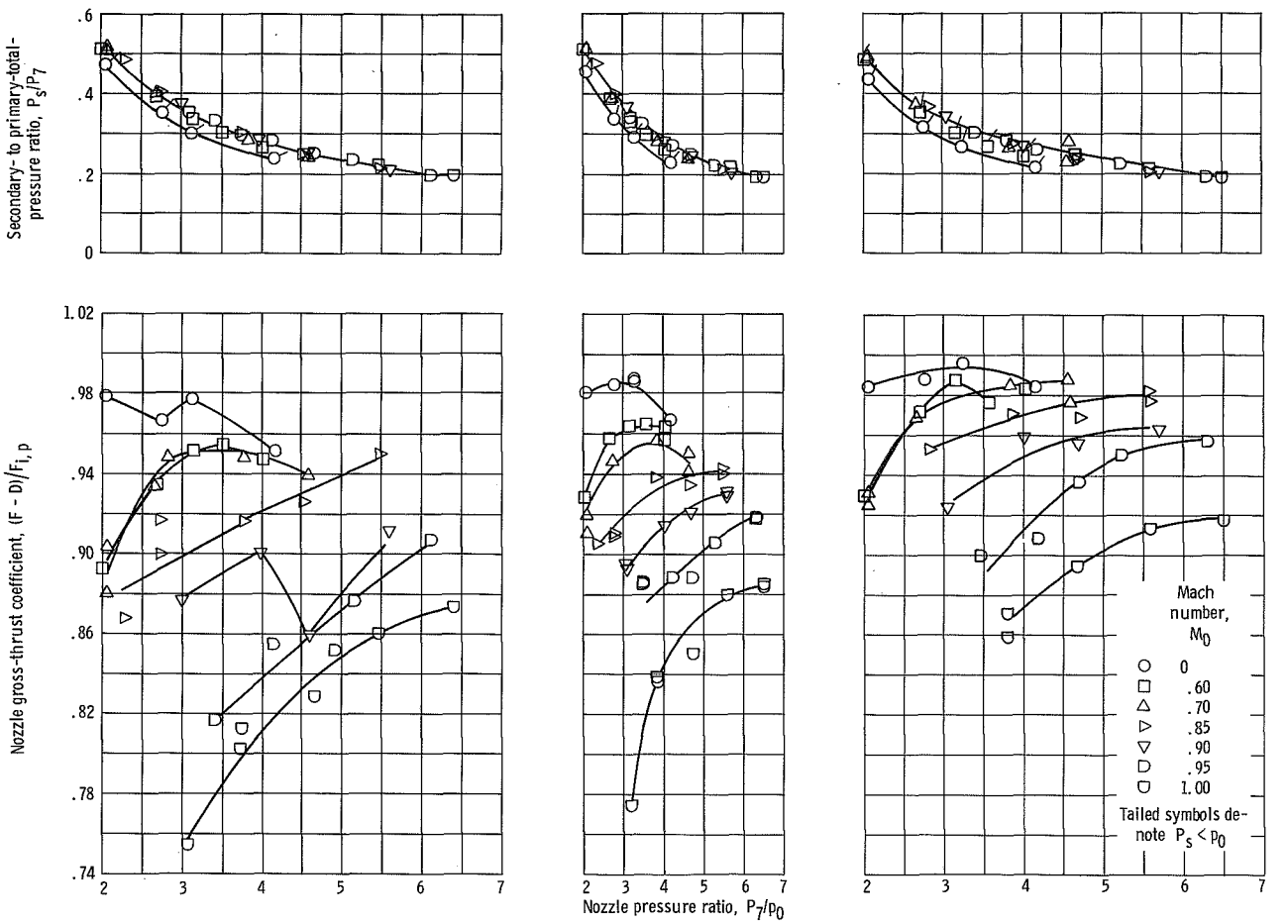

(a) 10°-20° inlet doors (A_{ter}/A_9 = 0.715).

(b) 8°-16° inlet doors (A_{ter}/A_9 = 0.584).

(c) 5°-10° inlet doors (A_{ter}/A_9 = 0.368).

Figure 26. - Effect of nozzle pressure ratio on nozzle performance characteristics; primary nozzle configuration I (A_9/A_8 = 1.99). Corrected secondary-weight-flow-rate ratio, $\omega\sqrt{\tau}$ = 0.026.

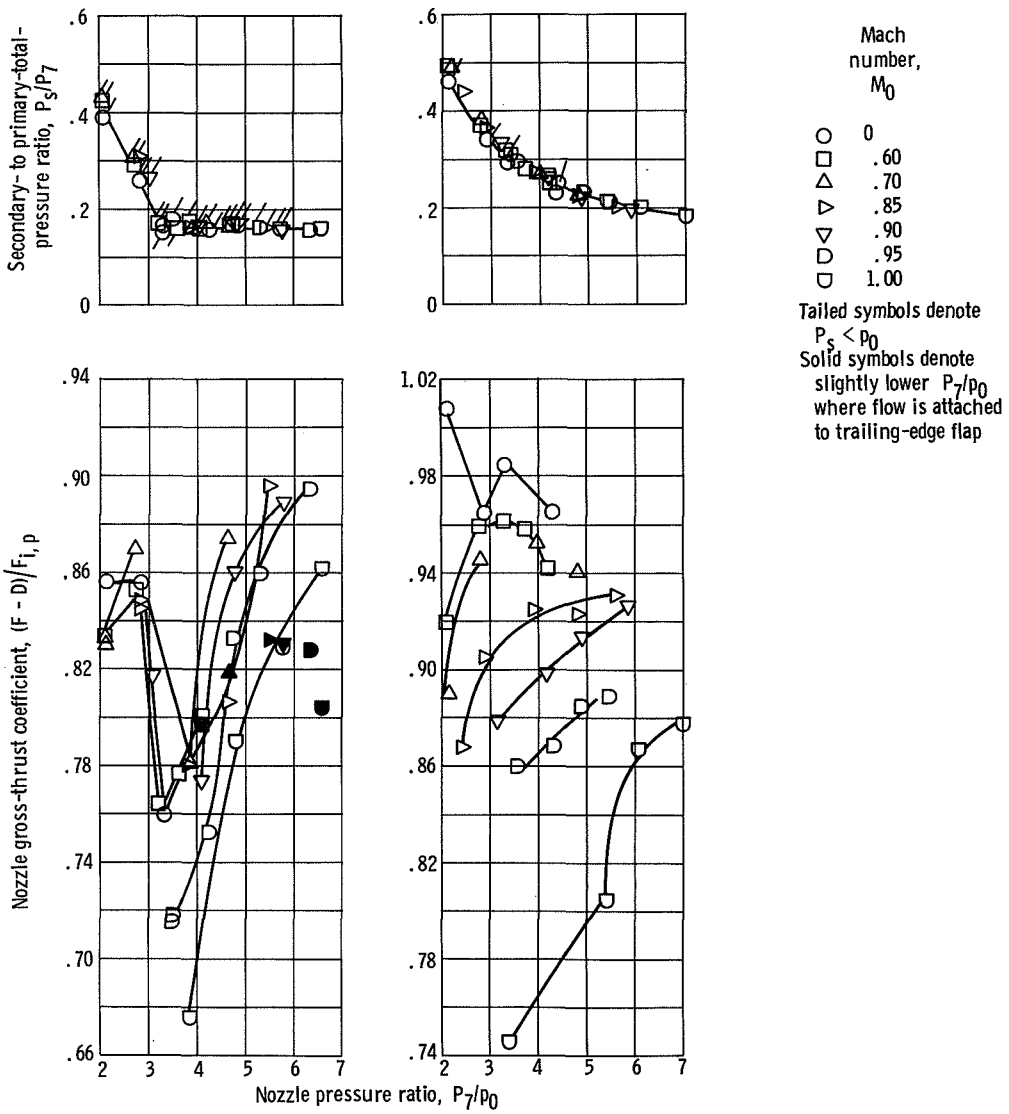

(d) Closed inlet doors ($A_{ter}/A_9 = 0$).

(e) 20° Inlet doors ($A_{ter}/A_9 = 0.715$).

Figure 26. - Continued.

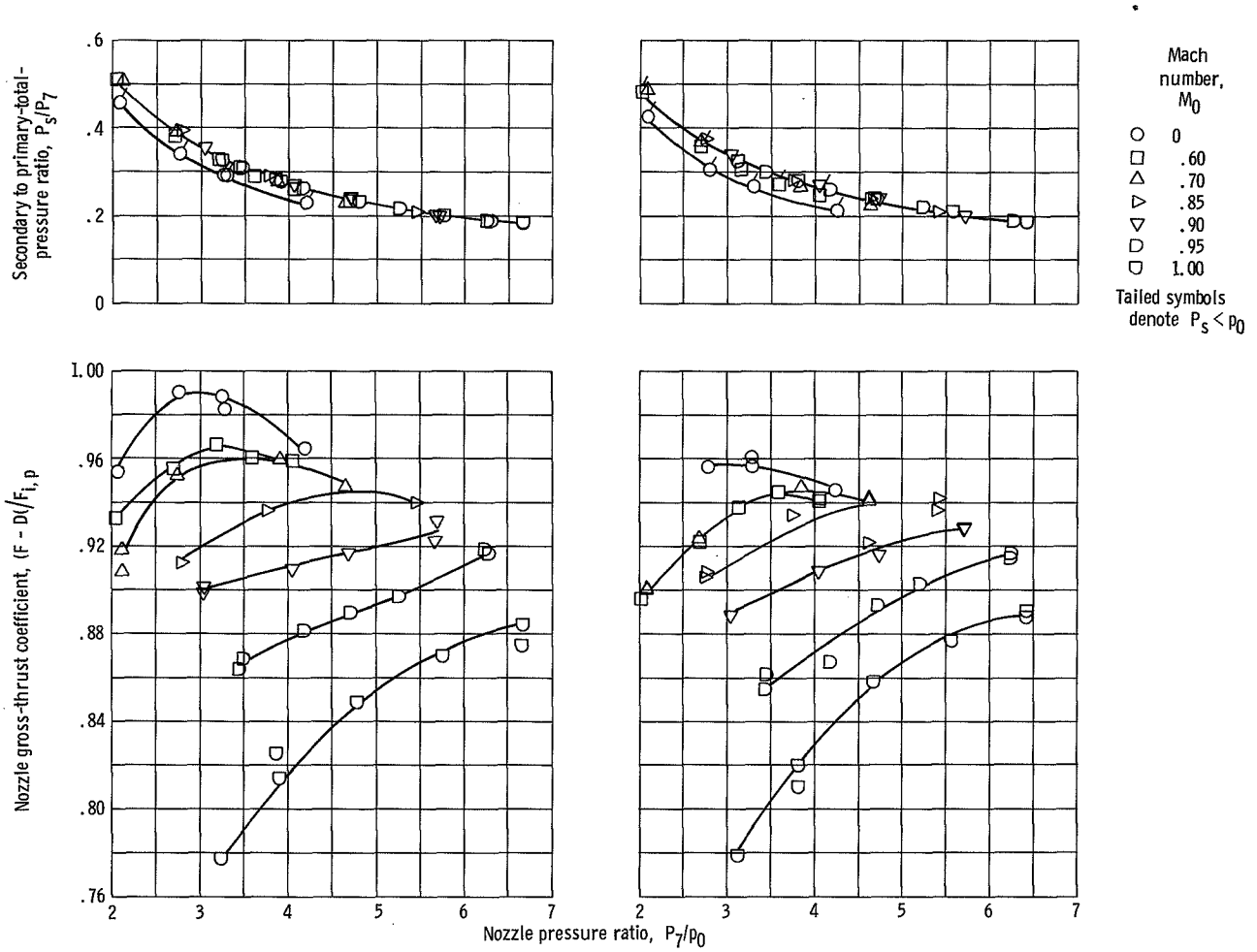

(f) 16° Inlet doors ($A_{ter}/A_9 = 0.584$).

(g) 10° Inlet doors ($A_{ter}/A_9 = 0.368$).

Figure 26. - Concluded.

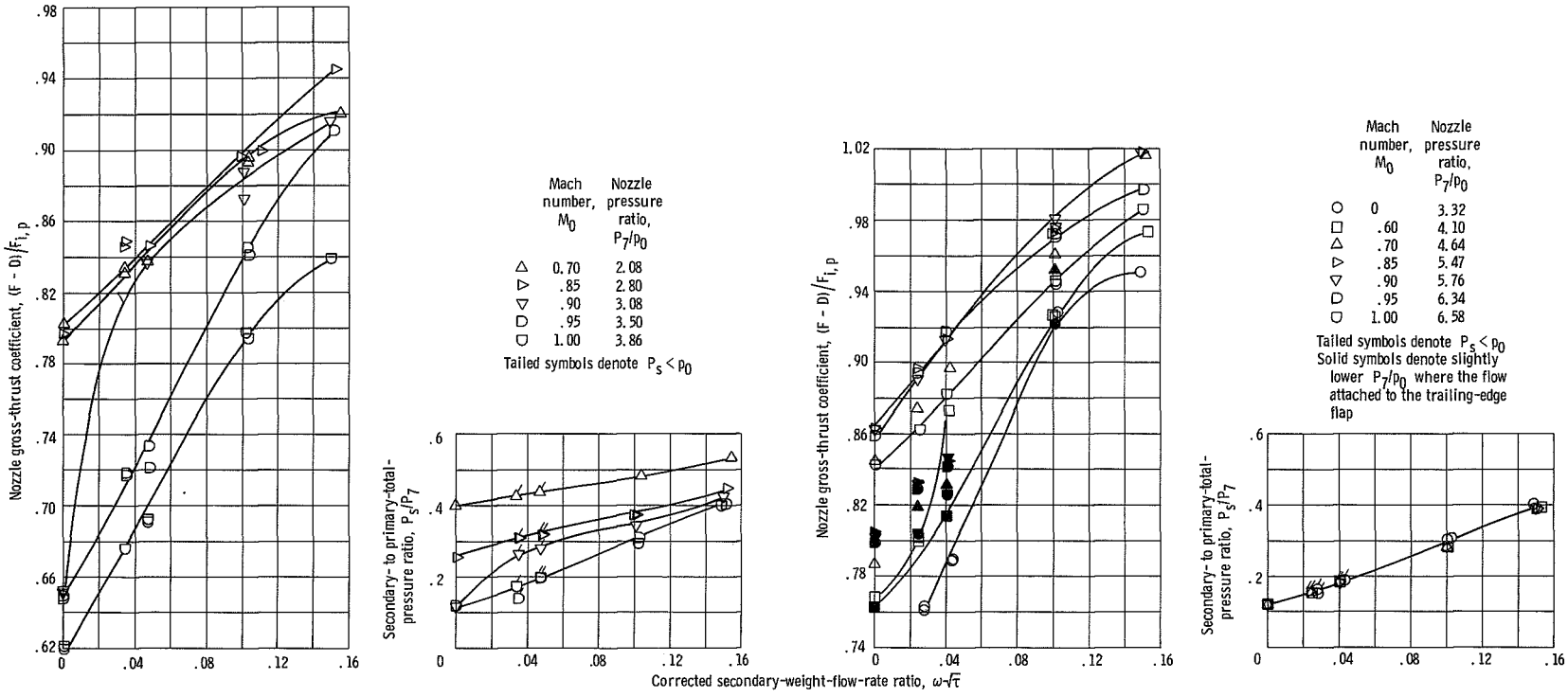

(a) Subsonic-cruise power setting; closed inlet doors (A_{ter}/A_9 = 0).

(b) Dry acceleration power setting; closed inlet doors (A_{ter}/A_9 = 0).

Figure 27. - Effect of corrected secondary-weight-flow-rate ratio on nozzle performance characteristics; primary nozzle configuration I (A_9/A_8 = 1.99).

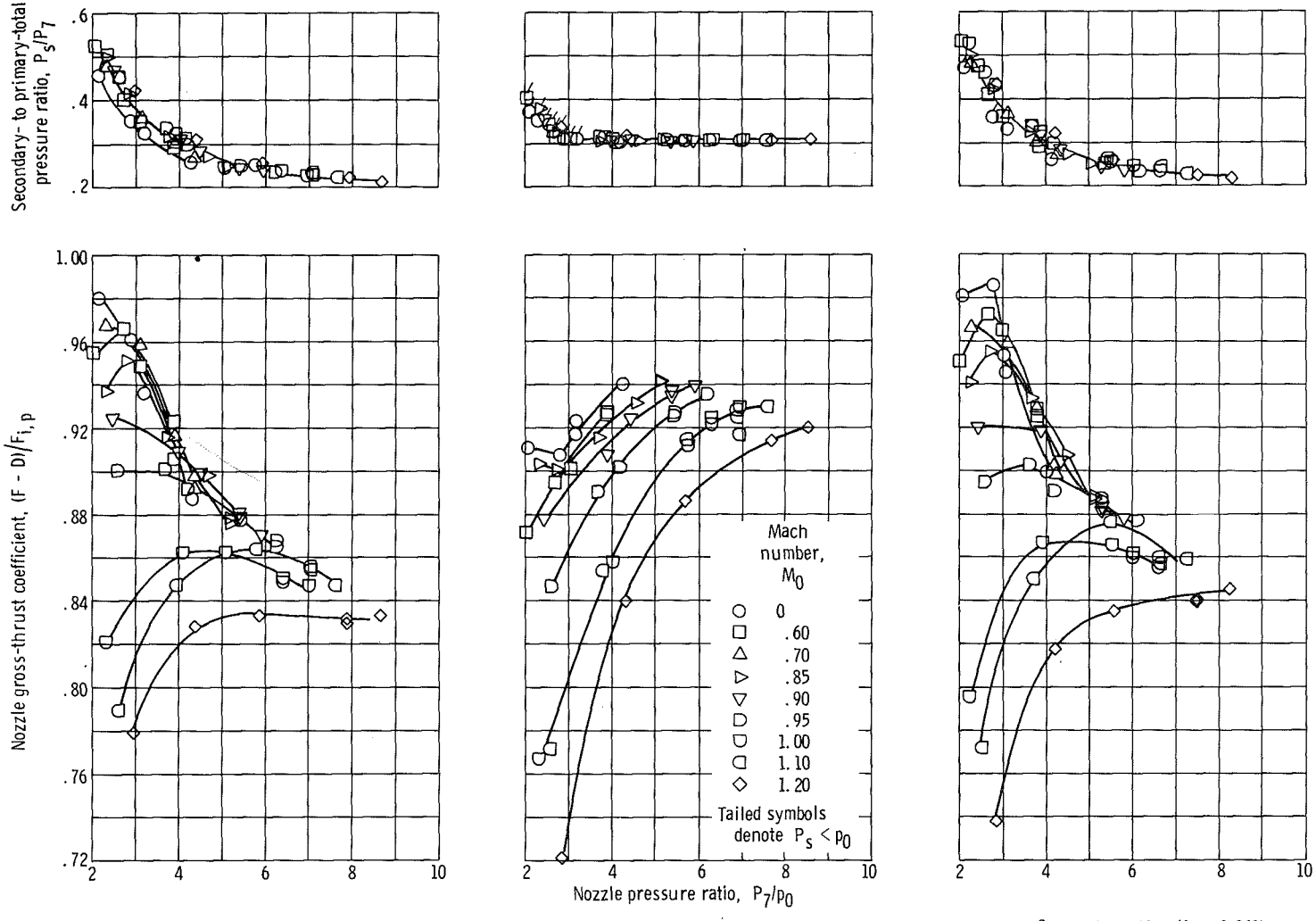

(a) 5°-10° inlet doors (A_{ter}/A_9 = 0.368).

(b) Closed inlet doors (A_{ter}/A_9 = 0).

(c) 10° inlet doors (A_{ter}/A_9 = 0.368).

Figure 28. - Effect of nozzle pressure ratio on nozzle performance characteristics; primary nozzle configuration II (A_9/A_8 = 1.42); corrected secondary-weight-flow-rate ratio, $\omega\sqrt{\tau}$ = 0.04.

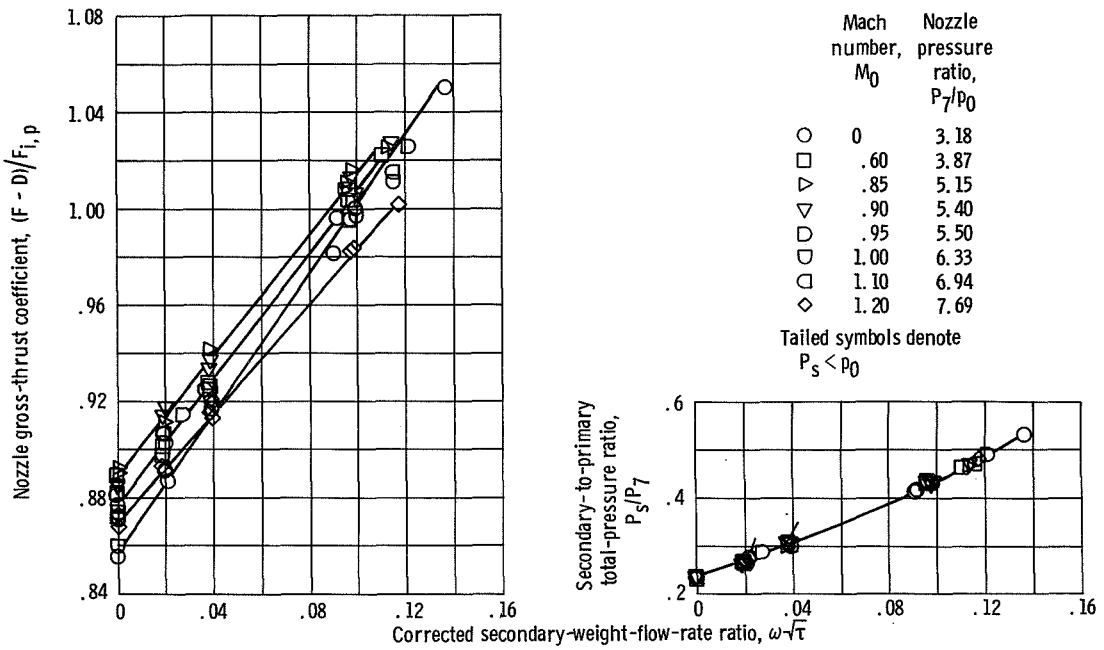

Figure 29. - Effect of corrected secondary-weight-flow-rate ratio on nozzle performance characteristics. Primary nozzle configuration II ($A_9/A_8 = 1.42$); closed inlet doors ($A_{ter}/A_9 = 0$).

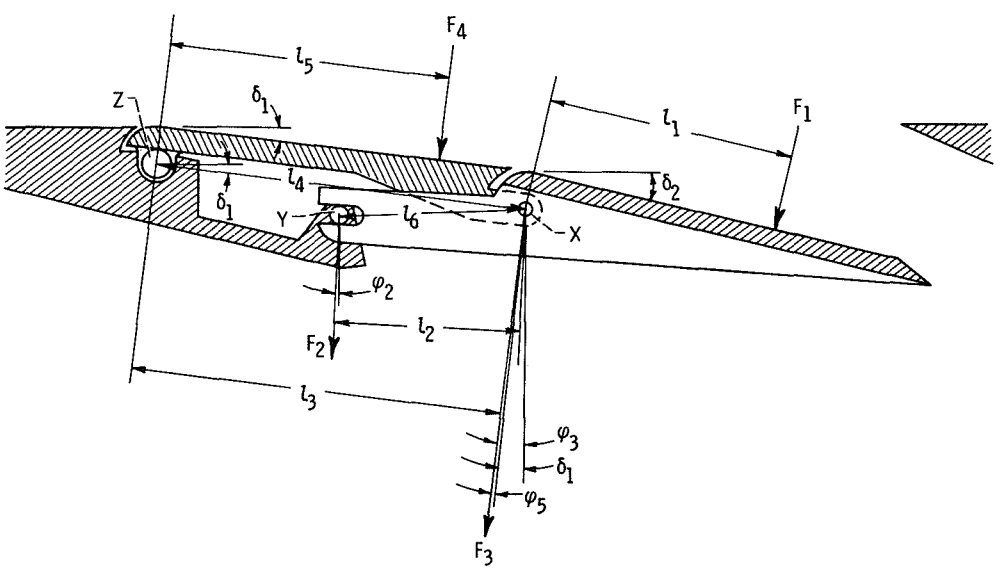

Figure 30. - Assumed mechanism for double-hinge door moment analysis.

"The aeronautical and space activities of the United States shall be conducted so as to contribute . . . to the expansion of human knowledge of phenomena in the atmosphere and space. The Administration shall provide for the widest practicable and appropriate dissemination of information concerning its activities and the results thereof."

—NATIONAL AERONAUTICS AND SPACE ACT OF 1958

NASA SCIENTIFIC AND TECHNICAL PUBLICATIONS

TECHNICAL REPORTS: Scientific and technical information considered important, complete, and a lasting contribution to existing knowledge.

TECHNICAL NOTES: Information less broad in scope but nevertheless of importance as a contribution to existing knowledge.

TECHNICAL MEMORANDUMS: Information receiving limited distribution because of preliminary data, security classification, or other reasons.

CONTRACTOR REPORTS: Scientific and technical information generated under a NASA contract or grant and considered an important contribution to existing knowledge.

TECHNICAL TRANSLATIONS: Information published in a foreign language considered to merit NASA distribution in English.

SPECIAL PUBLICATIONS: Information derived from or of value to NASA activities. Publications include conference proceedings, monographs, data compilations, handbooks, sourcebooks, and special bibliographies.

TECHNOLOGY UTILIZATION PUBLICATIONS: Information on technology used by NASA that may be of particular interest in commercial and other non-aerospace applications. Publications include Tech Briefs, Technology Utilization Reports and Notes, and Technology Surveys.

Details on the availability of these publications may be obtained from:

SCIENTIFIC AND TECHNICAL INFORMATION DIVISION

NATIONAL AERONAUTICS AND SPACE ADMINISTRATION

Washington, D.C. 20546